

CANCER

A biomimetic pancreatic cancer on-chip reveals endothelial ablation via ALK7 signaling

Duc-Huy T. Nguyen^{1*}, Esak Lee^{2,3*†}, Styliani Alimperti^{2,3}, Robert J. Norgard⁴, Alec Wong², Jake June-Koo Lee⁵, Jeroen Eyckmans^{2,3}, Ben Z. Stanger⁴, Christopher S. Chen^{1,2,3‡}

Pancreatic ductal adenocarcinoma (PDAC) is an aggressive, lethal malignancy that invades adjacent vasculatures and spreads to distant sites before clinical detection. Although invasion into the peripancreatic vasculature is one of the hallmarks of PDAC, paradoxically, PDAC tumors also exhibit hypovascularity. How PDAC tumors become hypovascular is poorly understood. We describe an organotypic PDAC-on-a-chip culture model that emulates vascular invasion and tumor–blood vessel interactions to better understand PDAC–vascular interactions. The model features a 3D matrix containing juxtaposed PDAC and perfusable endothelial lumens. PDAC cells invaded through intervening matrix, into vessel lumen, and ablated the endothelial cells, leaving behind tumor-filled luminal structures. Endothelial ablation was also observed in *in vivo* PDAC models. We also identified the activin-ALK7 pathway as a mediator of endothelial ablation by PDAC. This tumor-on-a-chip model provides an important *in vitro* platform for investigating the process of PDAC-driven endothelial ablation and may provide a mechanism for tumor hypovascularity.

INTRODUCTION

Although the diagnosis and treatment of cancer in its earliest stages has substantially improved outcomes in many tumors, survival rates in patients with tumors that have spread to distant sites remain dismal (1). Hence, the vast majority of cancer mortalities stem from metastasis and its complications (2). Metastasis is a final product of a chain of multiple complex steps, including local spread of cancer cells at primary sites of origin, invasive entry into nearby vasculature (intravasation), exit from vasculature (extravasation), and growth at distant organ sites (3). To complete the metastasis cascade, tumor cells need to extensively interact with the vasculature. However, the interactions between cancer cells and blood vessels in particular are poorly understood.

One of the many examples of poorly understood tumor-endothelium interactions is in pancreatic ductal adenocarcinoma (PDAC). PDAC is a highly metastatic cancer whose cancer cells have been shown to escape the tumor and enter the circulation at the very earliest stages of tumor progression (4, 5). The vast majority of patients once diagnosed with PDAC are already at the later stages of the disease (6). At the same time, tumor masses from these patients generally exhibit hypovascularity or a paucity of capillary vessels within these tumors (7). Hence, there is an unusual yet poorly understood transition in interactions between tumor and the blood vessels in PDAC: At early stages, nearby blood vessels are essential in providing a means for tumor cells to gain access to the circulation, but at later stages, they are absent and can limit chemotherapeutic drug delivery to the tumors. Thus, understanding these tumor-endothelium interactions within PDAC will provide important insights into PDAC tumor biology.

¹Department of Chemical and Biomolecular Engineering, University of Pennsylvania, Philadelphia, PA 19104, USA. ²Department of Biomedical Engineering, Boston University, Boston, MA 02215, USA. ³Wyss Institute for Biologically Inspired Engineering, Harvard University, Boston, MA 02115, USA. ⁴Division of Gastroenterology, Department of Medicine and Abramson Family Cancer Research Institute, Perelman School of Medicine, University of Pennsylvania, Philadelphia, PA 19104, USA. ⁵Department of Biomedical Informatics, Harvard Medical School, Boston, MA 02115, USA.

*These authors contributed equally to this work.

†Present address: Nancy E. and Peter C. Meinig School of Biomedical Engineering, Cornell University, Ithaca, NY 14853, USA.

‡Corresponding author. Email: chencs@bu.edu

In part, a lack of detailed understanding of tumor-vessel interactions in PDAC is due to difficulties in observing and studying these interactions in traditional models of tumor invasion. Although a few histologic studies of patient samples have observed the extensive invasion of tumor cells into the vasculature (8–10), follow-up *in vivo* studies in mice have not advanced our understanding of this phenomenon owing to the complexity of animal models (11) and challenges in spatiotemporal imaging of tumor-vessel interactions in internal organs, such as pancreas (12). Alternative to *in vivo* approaches, recent advances in microfluidic microphysiological systems have allowed the generation of blood vessel–tumor interfaces *in vitro* (13–18). Early studies using these *in vitro* cultures to model the interactions between tumor cells with two-dimensional (2D) planar or 3D vessel-like structures have demonstrated the value of juxtaposing tumor cells with the vascular compartment, especially in the context of investigating extravasation and intravasation properties (14, 15, 19–21). However, so far, these models have not been used to study interactions between malignant PDAC and blood vessels.

To achieve a deeper understanding of tumor-endothelium interactions in PDAC, we describe here a model system in which a biomimetic ductal channel containing PDAC cells is juxtaposed to a rudimentary blood vessel consisting of an endothelialized, perfused lumen. Using this model, we observed that PDAC tumor cells can invade and remove the vascular endothelium to leave behind tumor-lined and tumor-filled luminal structures, a process we refer to as endothelial ablation. We further validated our findings in *in vivo* PDAC models and identified a crucial role for activin-ALK7 signaling in mediating endothelial ablation in PDAC. On the basis of our studies, we propose that endothelial cell ablation by tumor cells via the activin-ALK7 signaling pathway may be a potential mechanism to explain hypovascularity in PDAC.

RESULTS

An organotypic model of PDAC exhibits 3D invasion and ablation of endothelial cells

To examine the process of PDAC invasion, we engineered an organotypic model of PDAC building on a previously developed

Copyright © 2019
The Authors, some
rights reserved;
exclusive licensee
American Association
for the Advancement
of Science. No claim to
original U.S. Government
Works. Distributed
under a Creative
Commons Attribution
NonCommercial
License 4.0 (CC BY-NC).

Downloaded from <http://advances.sciencemag.org/> on August 29, 2019

vessel-on-a-chip (18). Briefly, our PDAC organotypic model is composed of two hollow cylindrical channels, which are completely embedded into 3D collagen matrix (Fig. 1A). In one of the channels, we seeded endothelial cells to form a biomimetic blood vessel, as previously described (18). In a parallel channel, we seeded primary mouse pancreatic cancer cells PD7591 and allowed them to adhere to form a monolayer of epithelial cells to mimic a ductal compartment of a pancreatic duct. To study the interactions of PDAC cells with the blood vessels, we performed a screening experiment wherein different chemotactic agents were introduced into the biomimetic blood vessel and found that a gradient of fetal bovine serum (FBS) most efficiently stimulated invasion of pancreatic cancer cells into the collagen matrix (fig. S1, A to D). Characterization of the gradient using 21-kDa fluorescein isothiocyanate

dextran (FITC-dextran) showed a gradual loss in the steepness of the gradient (fig. S1E), prompting us to administer FBS daily in the endothelial channel to maintain the FBS gradient during the course of the experiments.

Upon stimulation with FBS, the PDAC cells in the biomimetic ductal channel began to proliferate to form a multilayer of cells (fig. S2). By day 4, PD7591 cells began to invade into the matrix toward the endothelial lumen. The invasion was collective, with epithelial cells remaining in contact with each other, to form branched structures reminiscent of epithelial morphogenesis (Fig. 1B). The presence of the endothelium increased the migration speed of PD7591 in response to the FBS gradient (Fig. 1B), until reaching the engineered blood vessel. Upon contact with the biomimetic blood vessel, the PDAC cells wrapped around the blood vessel and spread along the

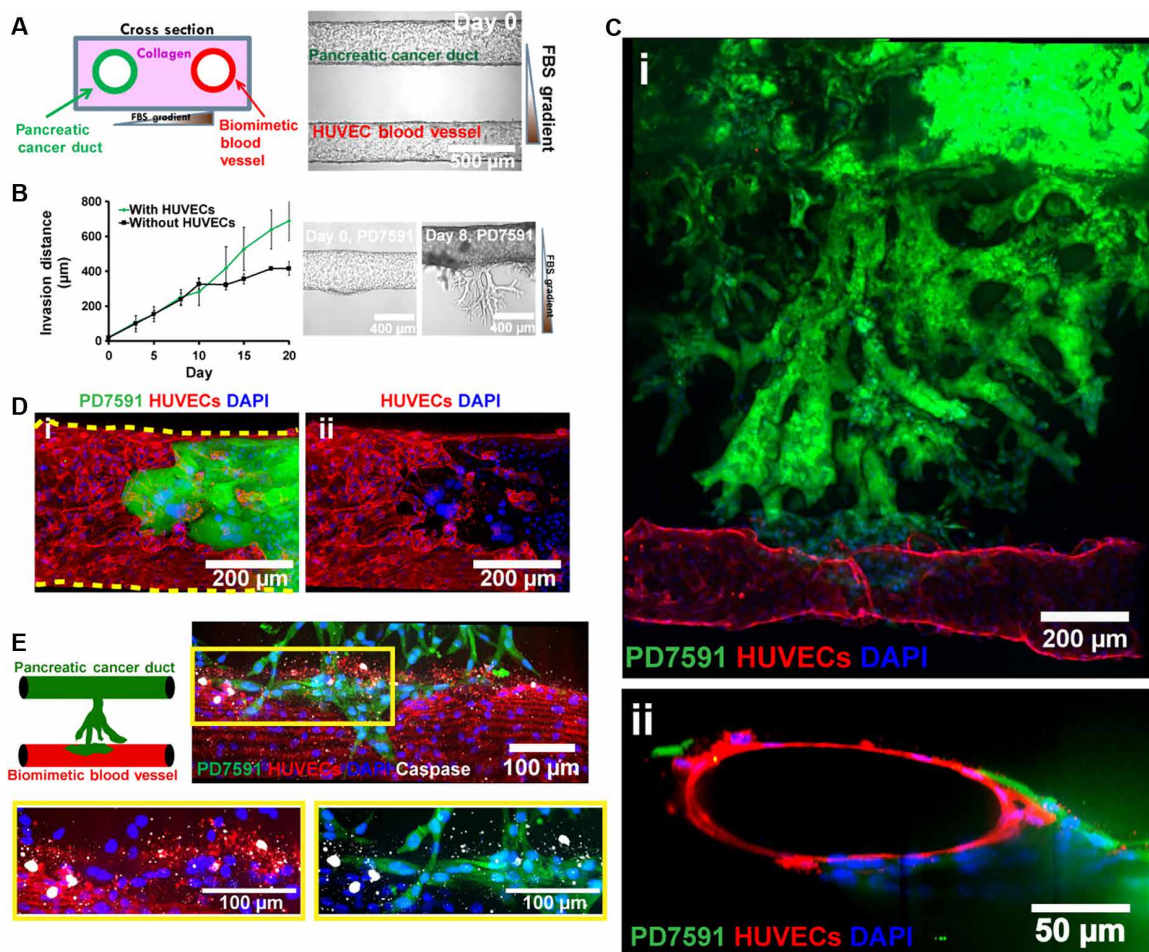


Fig. 1. Organotypic model for PDAC-on-a-chip to capture pancreatic tumor vascular invasion. (A) Schematic of PDAC-on-a-chip with a biomimetic blood vessel and a pancreatic cancer duct. The microfluidic device is composed of two hollow cylindrical channels embedded within 3D collagen matrix. One channel was seeded with endothelial cells to form a perfusable biomimetic blood vessel, while the other channel was seeded with pancreatic cancer cells to form a pancreatic cancer duct. Phase-contrast image shows seeded cells in the device before PDAC migration. (B) Average invasion distance of a PDAC cell line, YFP PD7591, toward a gradient of FBS with and without human umbilical vein endothelial cells (HUVECs). The presence of HUVECs increased the migration speed of PD7591 ($n = 3$ individual experiments). Representative phase-contrast images of PD7591 migration at days 0 and 8 demonstrated the collective migration of PDAC invasion. (C) YFP PD7591 (in green) invaded toward the biomimetic blood vessel (in red), migrated along the vessel (i), and wrapped around the blood vessel, as shown in the cross-sectional image of the biomimetic blood vessel (ii). (D) A confocal image of a section of the blood vessel (in red) invaded by YFP PD7591 (in green) showed that part of the blood vessel was ablated by cancer cells in our organotypic model (i and ii). (E) Apoptosis, marked by cleaved caspase-3 staining (in white), was observed in endothelial cells (in red) during invasion of YFP PD7591 (in green) in the blood vessels in our 3D PDAC organotypic model. Endothelial cells in all images were stained with anti-CD31 antibody. YFP PD7591 was retained with FITC-conjugated anti-GFP (green fluorescent protein) antibody. Cell nuclei were stained with 4',6-diamidino-2-phenylindole (DAPI) (in blue). Error bars are SEM.

length of the blood vessel before invading into the vessel itself (Fig. 1C, i and ii, and movie S1).

During PD7591 invasion into the blood vessel, we observed that part of the blood vessel was occupied by the tumor PD7591 cells (Fig. 1D, i and ii, and movie S2), a finding that was replicated with three additional primary mouse PDAC cell lines and a human pancreatic cancer cell line (fig. S3). As the PDAC cells invaded and occupied the lumen of the biomimetic blood vessels, we also observed apoptotic endothelial cells in proximity to the PDAC cells (Fig. 1E), whereas endothelial cells in the biomimetic blood vessels without tumor invasion exhibited no apoptotic activity (fig. S4A). In our 3D organotypic model, our endothelium deposited a collagen IV layer, while the PDAC cells in the biomimetic pancreatic cancer duct did not deposit collagen IV (fig. S4B). We also observed that, as the tumor cells ablated the endothelial cells in the 3D biomimetic blood vessel, the collagen IV layer deposited by the endothelium gradually disappeared (fig. S4C). We collectively refer to this process as endothelial ablation, where the PDAC tumor cells invade the blood vessels and ablate the endothelial cells, leaving behind tumor-lined and tumor-filled luminal structures.

Endothelial ablation is observed in vivo tumor models of PDAC

To verify that the used tumor cells PD7591 also ablated endothelial cells in vivo and further confirm that the biomimetic model reproduces an in vivo process that occurs in pancreatic cancers, we subcutaneously inoculated the same tumor cells into mice. After the tumor volume reached approximately 400 mm³, we resected the tumor, including the adjacent area around the tumor, for analysis. Immunohistochemical staining for cleaved caspase-3 and CD31 showed that endothelial cells were apoptotic in the PDAC tumor in vivo (Fig. 2A). In contrast, control mice injected with Matrigel alone had a minimal amount of apoptotic endothelial cells (fig. S5A). Because tumor cells PD7591 did not deposit collagen IV in our in vitro and in vivo experiments (fig. S4, B and D), while blood vessels in vivo were surrounded by collagen IV (fig. S4, E and F), we stained for endomucin or CD31 as endothelial cell markers and collagen IV (a basement membrane protein in vessels) to identify blood vessels in PDAC tumors. A subset of vessel lumens in the tumor-containing regions was mosaically lined by both endothelial and PDAC cells (Fig. 2B, red arrows), and several collagen IV-lined lumens, reminiscent of blood vessels, were lined luminally with only PDAC cells (Fig. 2B, yellow arrows). These data are aligned with our in vitro findings (Fig. 1, D and E), therefore suggesting that our biomimetic model of PDAC captures a relevant in vivo process of PDAC progression.

To further strengthen our finding of endothelial ablation in PDAC in vivo, we sought to demonstrate the presence of blood vessels occupied by tumor cells in a genetically engineered mouse model (GEMM) of PDAC, in which many aspects of human tumor biology and progression are captured (22). In this GEMM, tumor cells were genetically tagged with a yellow fluorescent protein, and PDAC tumor tissue sections were immunohistochemically stained for endomucin and collagen IV to highlight the endothelium and their basement membrane protein. Similar to the ectopic model, tumor cells in the GEMM were also found at the luminal side of blood vessels (Fig. 2C). Together, our findings in both in vivo tumor mouse models and our 3D biomimetic model suggest that PDAC invades blood vessels, gains access to the luminal space of the blood

vessels, and ultimately ablates the endothelium to form tumor cell-lined luminal structures, a process that may contribute to the hypovascularity observed in larger PDAC tumor masses.

Endothelial ablation in PDAC is mediated through a transforming growth factor- β receptor signaling pathway

We next sought to identify which signaling pathways were involved in endothelial ablation. The transforming growth factor- β (TGF- β) signaling pathway has been implicated in tumor progression in many different types of tumors, including PDAC (23). We therefore asked whether the TGF- β receptor signaling pathway was involved in endothelial ablation in PDAC. Using our 3D organotypic model, we allowed pancreatic cancer cells from the pancreatic cancer duct to invade the engineered blood vessel. Once the pancreatic cancer cells reached the blood vessels, we initiated treatment with SB431542 at 5 μ M for a duration of 7 days. We observed that inhibition of TGF- β receptor signaling significantly reduced the ablation of endothelial cells by pancreatic cancer cells in our biomimetic blood vessel (Fig. 3A, i and ii, and fig. S8, A and B). Quantification of the endothelial cell vessel area that was ablated by PDAC cells further confirmed our observation (Fig. 3A). Western blot of phosphorylated Smad2 confirmed the effect of SB431542 inhibition on TGF- β receptor signaling in both endothelial cells and PD7591 (Fig. 3A).

We further investigated whether inhibition of TGF- β receptor signaling also led to reduced endothelial ablation in vivo by subcutaneously injecting the same pancreatic cancer cell line PD7591 into mice. By day 9, when the tumor reached 100 mm³, we administered SB431542 versus control vehicle into two groups of mice through daily peritoneal injections for 1 and 2 weeks. In tumors harvested from SB431542-treated mice, we measured a higher density of vessels by quantifying the CD31 signal intensity within the tumor microenvironment (Fig. 3B and fig. S5B). We also noticed a minimal proliferation of endothelial cells in both control and SB431542-treated tumors (fig. S5C), indirectly suggesting that the increase in CD31 signal intensity in SB431542-treated tumors was likely due to less endothelial cell ablation. Similarly, quantification of cleaved caspase-3 signal intensity showed a less apoptotic signal in endothelial cells in SB431542-treated mice at 1 and 2 weeks versus control mice. However, endothelial cell ablation and apoptosis were not fully inhibited, as the apoptotic caspase signal was still higher at 2 weeks versus 1 week. Of note, the tumor growth rate was not affected by administration of SB431542 in vivo (fig. S5D). Together, our in vitro and in vivo data suggested that inhibiting TGF- β receptor signaling reduces endothelial ablation in PDAC.

Endothelial ablation of PDAC is mediated through an activin-ALK7 pathway

Because SB431542 has previously been reported as a broad inhibitor for the TGF- β superfamily receptors ALK4, ALK5, and ALK7 (24), we sought to determine which of these receptors in each of the cell types might contribute to endothelial ablation. To address this question, we designed a simple 2D patterned coculture invasion assay to quickly enable us to identify the molecular mechanism of endothelial cell ablation. Briefly, PDAC cells were plated inside a silicone annulus, while endothelial cells were plated outside the annulus. Peeling the annulus off the substrate left a circular population of PDAC cells surrounded by a monolayer of endothelial cells (Fig. 4A). As time progressed, the PDAC cells invaded into the endothelial cell area and ablated the endothelial cells (movie S3),

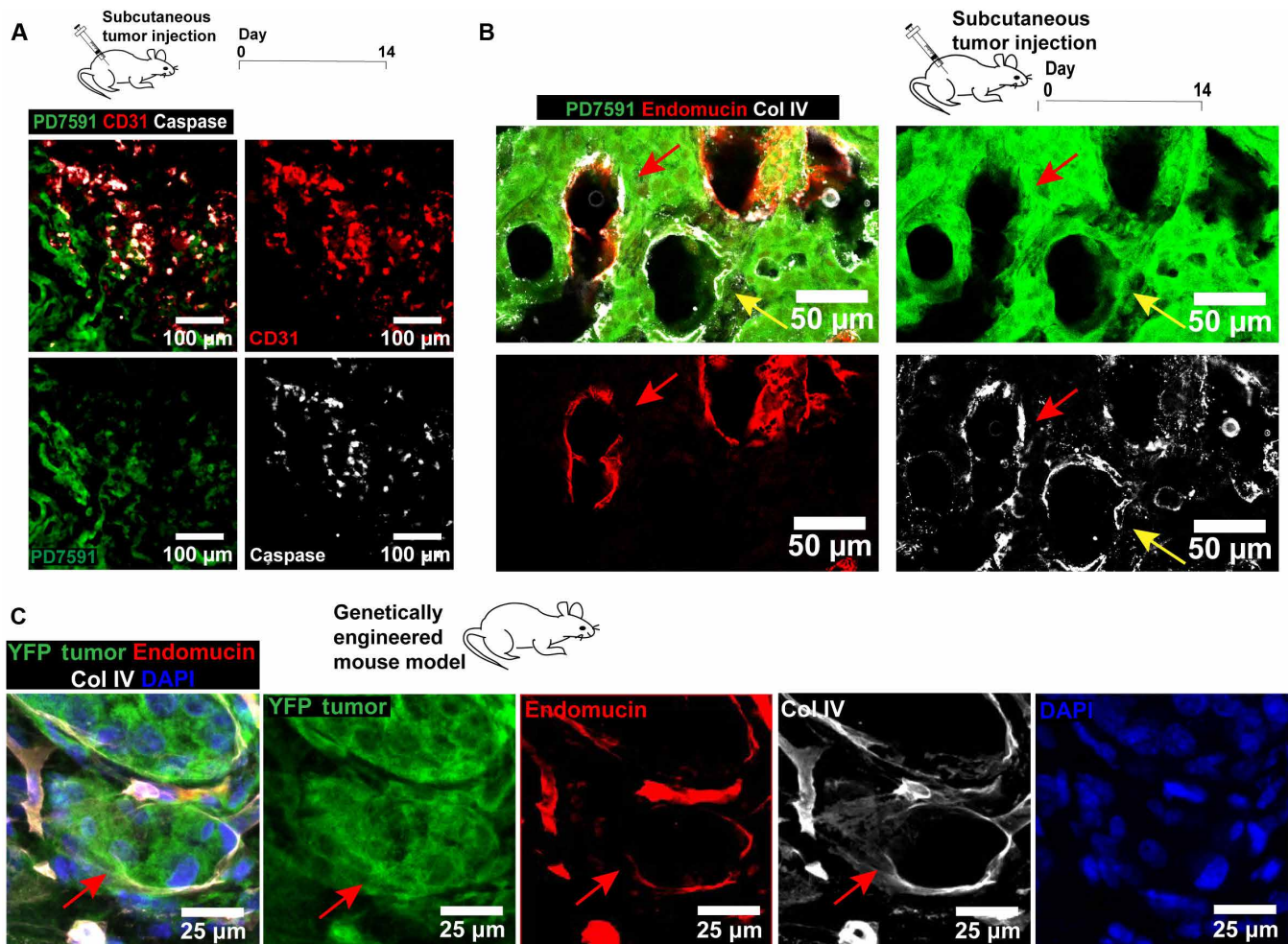


Fig. 2. Endothelial ablation is observed in in vivo mouse tumor models (subcutaneous tumor implantation model and genetically engineered mouse model). (A) Examination of endothelial cells in the ectopic mouse tumors in vivo. YFP PD7591 (in green) was subcutaneously injected into mice for 14 days. Apoptotic endothelial cells were also observed in the in vivo tumor microenvironment, similarly to the observation in the 3D organotypic model. Apoptotic endothelial cells (in red) were marked by cleaved caspase-3 signal (in white). (B) Endothelial ablation in subcutaneous tumor implantation model. Resected tumors at day 14 exhibited partial ablation of endothelial cells by pancreatic cancer cells (red arrows) in hybrid blood vessels. Some small vessels, decorated with collagen IV (in white), a basement membrane protein, demonstrated complete endothelial ablation by YFP PD7591 in the luminal side of the vessels (yellow arrows). Blood vessels were stained with anti-mouse endomucin antibody (in red). (C) Endothelial ablation was observed in GEMM of PDAC. Partial ablation of endothelium in the blood vessel was indicated by red arrows, where the blood vessel displayed the occupation of yellow fluorescent protein (YFP) tumor cells in place of the endothelium. Endothelial cells in all images were stained with either anti-mouse CD31 antibody or anti-mouse endomucin. YFP PD7591 was restained with FITC-conjugated anti-GFP antibody. Cell nuclei were stained with DAPI (in blue).

resulting in an increase in the area of PDAC cells (Fig. 4B and fig. S9A). When SB431542 was added into the coculture of PD7591 and endothelial cells, the PDAC invasion area was significantly decreased (Fig. 4B, fig. S9B, and movie S4), resembling the effects of blocking the TGF- β receptor signaling pathway to prevent endothelial ablation in our 3D organotypic model. We further showed the effects of inhibiting the TGF- β receptor signaling pathway to reduce endothelial ablation in two other human pancreatic cancer cell lines (Panc-1 and BxPC-3; fig. S6, A and B).

Using this 2D patterned coculture invasion assay, we first stained for cleaved caspase-3 activity to examine whether apoptosis coincided with PDAC invasion of the endothelial cell area. In agreement with our findings in the 3D organotypic model, the cleaved caspase-3 signal was only detected in endothelial cells, and the cleaved caspase-3 signal intensity in endothelial cells was the highest at the interface between endothelial and tumor cells and dropped as the endothelial

cells were further away from the interface (fig. S6C). Administration of SB431542 significantly reduced the number of apoptotic endothelial cells, particularly at the interface between endothelial and cancer cells (fig. S6C), suggesting that direct contact between endothelial and PDAC cells may be required for endothelial ablation. To test this hypothesis, we monitored the endothelial-PDAC interface using time-lapse microscopy and found that endothelial cells begin to round up and detach from the substrate, two characteristics that are reminiscent of apoptosis, 8 hours after contact with the invading tumor cells (fig. S6D). Treatment of an endothelial monolayer with tumor-conditioned medium did not increase apoptosis, suggesting that the apoptotic signal is not soluble (fig. S7A). In contrast, endothelial cell ablation was reduced when proliferation of tumor cells was inhibited with aphidicolin (fig. S7B). Together, these data suggest that proliferation of the tumor cells and direct contact between endothelial and tumor cells are required for endothelial cell ablation to occur.

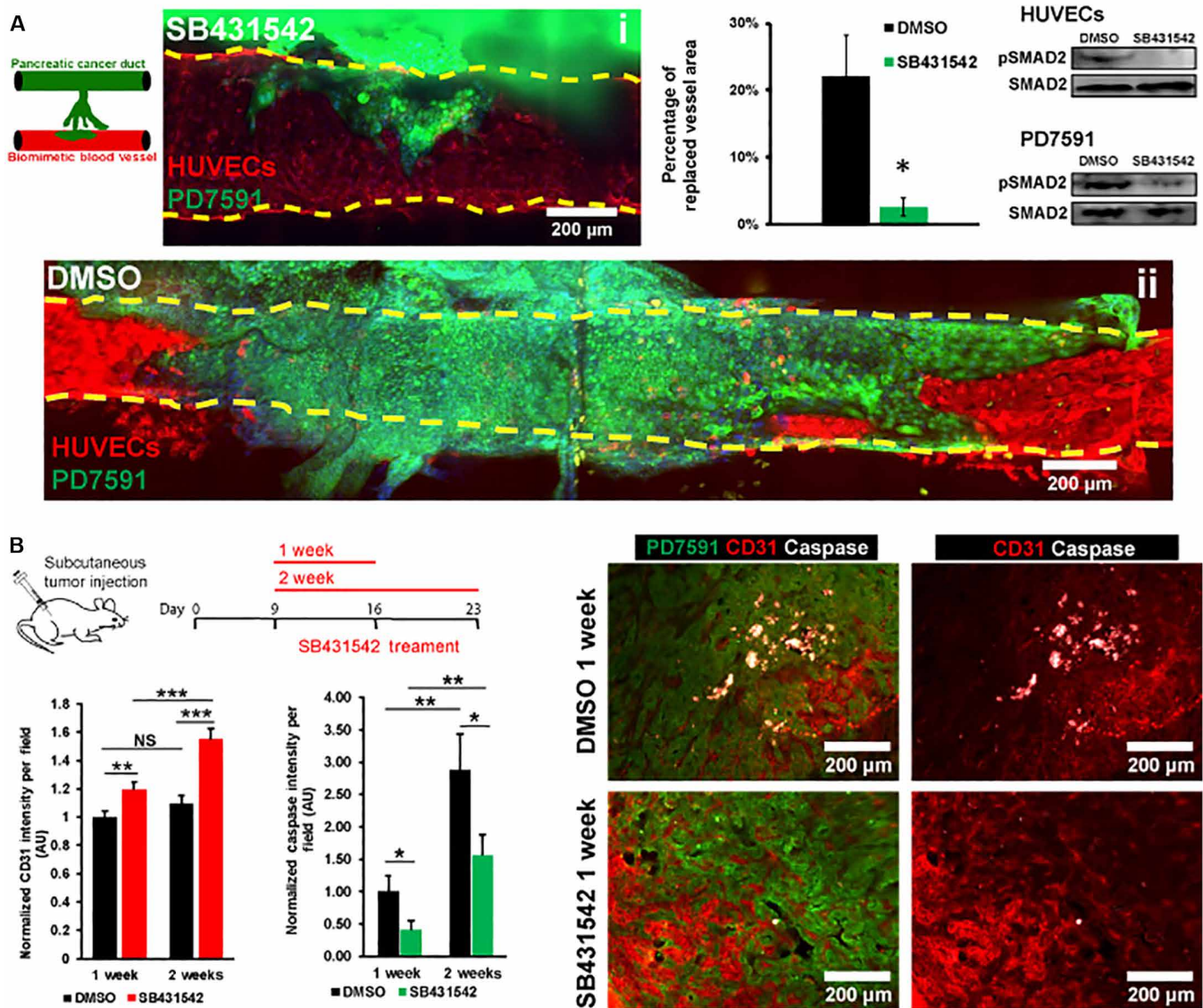


Fig. 3. Inhibition of the TGF- β receptor signaling pathway significantly reduced endothelial ablation. (A) Inhibition of TGF- β receptor signaling pathway with SB431542 in 3D organotypic model. PDAC tumor cells from the pancreatic cancer duct were allowed to invade into the biomimetic vessels. Once the PDAC tumor cells reached the blood vessels, 5 μ M SB431542 or dimethyl sulfoxide (DMSO) was administered for 7 days. Representative confocal images of vessels treated with SB431542 (i) and DMSO (ii) in 3D organotypic model. The percentage of endothelium-ablated area showed that SB431542 significantly reduced the endothelial ablation in 3D organotypic model ($n = 4$ individual experiments). Western blot for phosphorylated Smad2 in endothelial cells and PD7591 in 2D monoculture confirmed the effectiveness of SB431542 to inhibit the TGF- β signaling pathway in endothelial cells and in pancreatic cancer cells PD7591. (B) Inhibition of TGF- β receptor signaling pathway with SB431542 in a mouse tumor model for either 1 or 2 weeks. SB431542 was peritoneally administered into the mice daily for 1 and 2 weeks. Mice were sacrificed at days 16 and 23. Quantification of endothelial cell density revealed a significantly higher endothelial cell density within the tumors treated with SB431542 as compared to vehicle control ($n = 5$ mice per experimental group) for both 1 and 2 weeks. Cleaved caspase-3 activity in endothelial cells was also less in SB431542-treated tumors versus control tumors in both 1 and 2 weeks. Cleaved caspase-3 activity was significantly increased in tumors treated with SB431542 for 2 weeks versus 1 week. Right: Representative images of tumor samples in vehicle control DMSO and SB431542 conditions for 1-week condition. Endothelial cells were stained with anti-mouse CD31 antibody. YFP PD7591 was retained with FITC-conjugated anti-GFP antibody. Cell nuclei were stained with DAPI (in blue). * $P < 0.05$, ** $P < 0.01$, and *** $P < 0.001$ indicate statistical significance. NS, not significant. Two-tailed Student's *t* test. Error bars are SEM.

Because SB431542 exerted its effects in both endothelial and PDAC cells, we first used this system to investigate whether ALK4, ALK5, or ALK7 in endothelial cells played a role in endothelial ablation. We genetically deleted receptors ALK4, ALK5, and ALK7 in the endothelial cells using CRISPR-Cas9 technology and plated wild-type PD7591 and ALK4, ALK5, or ALK7 knockout human

umbilical vein endothelial cells (HUVECs) in the 2D patterned coculture invasion assay. Unexpectedly, the quantified invasion area of PD7591 showed no significant difference between ALK4, ALK5, or ALK7 knockout and scramble HUVEC conditions (fig. S7, C to E). Knockout of ALK4, ALK5, and ALK7 also did not affect the population doubling time of endothelial cells (fig. S7F). These

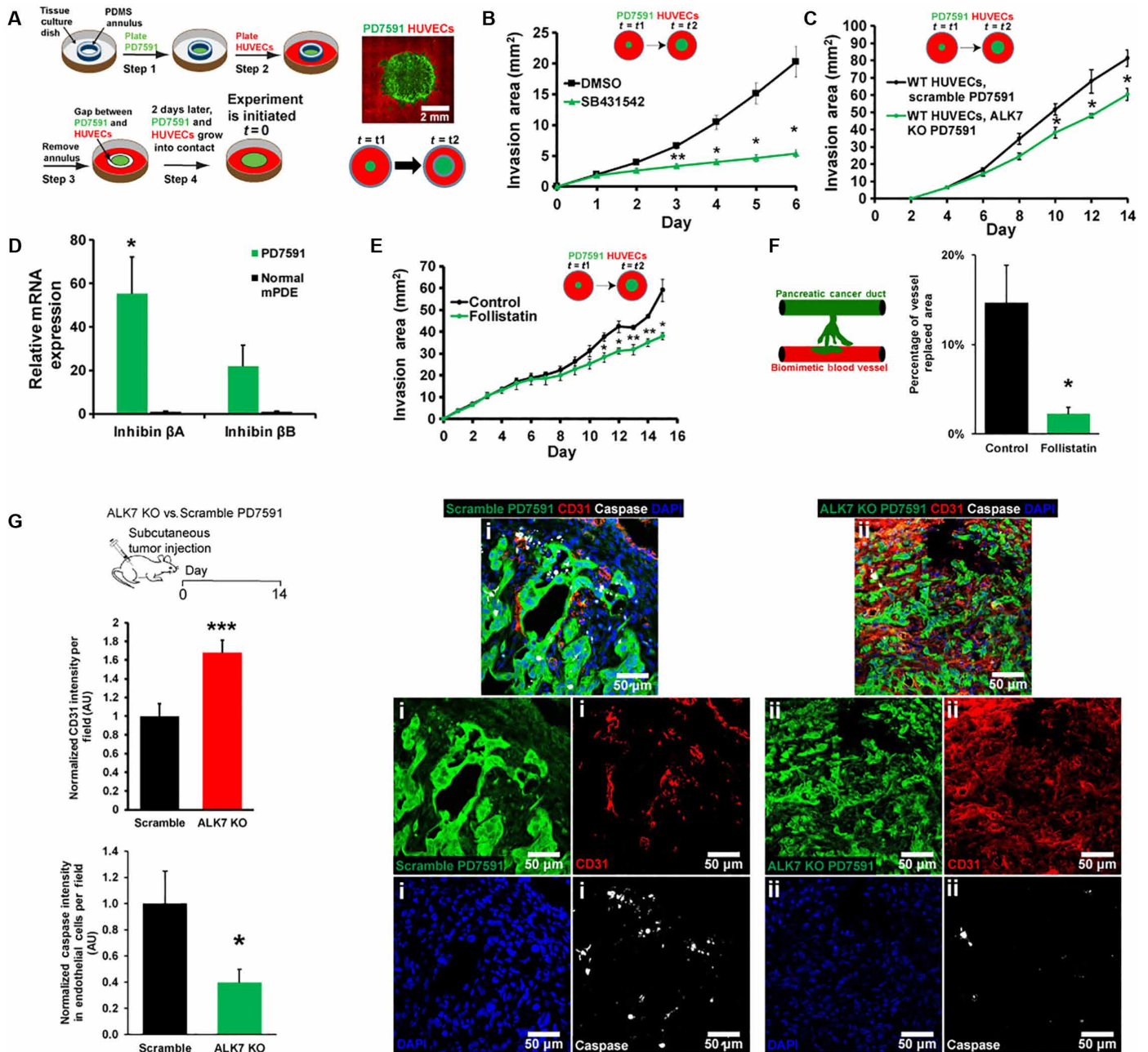


Fig. 4. Endothelial ablation required activin-ALK7 signaling in the invasive PDAC. (A) A schematic demonstrates a setup for 2D patterned coculture of PDAC and endothelial cells. Tumor cells were plated inside an annulus, and endothelial cells were plated outside the annulus. Once the annulus was removed, tumor invaded into the endothelial cells, resulting in an expansion of the tumor area. (B) SB431542 reduced endothelial ablation in 2D patterned coculture ($n = 3$ individual experiments). (C) ALK7 was knocked out in YFP PD7591 by CRISPR-Cas9 and plated in 2D patterned cocultures with wild-type (WT) HUVECs. Invasion area of ALK7 knockout (KO) YFP PD7591 was significantly less than scramble PD7591, suggesting the role of ALK7 in PD7591 to mediate endothelial ablation ($n = 3$ individual experiments). (D) Inhibin β A and inhibin β B, major subunits of activins, were up-regulated in pancreatic cancer cells as compared to normal mouse pancreatic ductal epithelial cells (mPDE) ($n = 3$ individual experiments). (E) Inhibition of activin with the endogenous inhibitor follistatin significantly diminished endothelial ablation of PDAC in 2D patterned cocultures ($n = 3$ individual experiments). (F) Inhibition of activin by follistatin (200 ng/ml) in 3D organotypic model revealed a significant reduction in tumor replaced blood vessel ($n = 3$ individual experiments). (G) In vivo mouse tumor model to confirm the role of ALK7 in endothelial ablation. ALK7 knockout PD7591 versus scramble cells were subcutaneously implanted into mice for 2 weeks. Cleaved caspase-3 signal indicated a substantial reduction in apoptotic endothelial cells in ALK7 knockout condition versus scrambled PD7591 condition ($n = 5$ mice per experimental group). A significant increase in endothelial cell density was also observed with ALK7 knockout PD7591 tumors versus scramble PD7591 tumors ($n = 5$ mice per experimental group). (i) Representative images of tumors implanted with scramble PD7591 depicted less endothelial cell density and high apoptotic signal. (ii) Representative images of tumor implanted with ALK7 knockout PD7591 depicted high endothelial cell density and less apoptotic signal. * $P < 0.05$, ** $P < 0.01$, and *** $P < 0.001$ indicate statistical significance. Two-tailed Student's t test. Error bars are SEM.

data strongly suggested the involvement of the TGF- β superfamily receptors in pancreatic cancer cells rather than in endothelial cells.

When ALK7 was knocked out in PD7591 cells, cellular invasion and endothelial ablation of PD7591 in 2D patterned cocultures (Fig. 4C and fig. S7H) were significantly reduced, while CRISPR-mediated knockout of ALK5 in PD7591 cells did not reduce endothelial ablation (fig. S7I). Knockout of ALK4 was not possible in these cancer cells despite multiple attempts with different guide RNA sequences, suggesting a requirement for ALK4 in these cells. Knockout of ALK7, but not ALK5, significantly prolonged the doubling time of PD7591 (fig. S7G), further supporting the notion that proliferation of tumor cells is likely involved in endothelial cell ablation.

Next, we sought to identify the ligand for the ALK7 signaling, as ALK7 can be activated via different ligands, such as nodal and activin. The major subunits of activin (inhibin β A and β B), in particular, were found to be highly up-regulated in the PDAC cells as compared to the normal mouse pancreatic ductal epithelial cells (Fig. 4D). We then exposed PDAC cells to follistatin, a naturally occurring activin inhibitor (25), in our 2D patterned coculture and in our 3D organotypic model. Inhibition of activin resulted in a significant reduction in endothelial ablation in 2D (Fig. 4E) and in a reduction of vessel replaced area in the 3D organotypic model (Fig. 4F and fig. S8, C and D), suggesting the involvement of activin in ALK7 activation during the process of endothelial ablation.

To further confirm the role of ALK7 in endothelial ablation, we knocked out ALK7 expression in PD7591 and subcutaneously implanted these tumor cells into mice. Tumors were allowed to grow for 2 weeks before they were resected. These tumors exhibited slower growth compared to control tumors (fig. S5E). Two weeks after tumor implantation, the tumors were resected and examined for vessel density and apoptotic endothelial cells. The ALK7-deficient tumors displayed a significantly higher vessel density and less apoptotic endothelial cells within the tumor mass as compared to scramble-treated control mice (Fig. 4G). Together, our *in vitro* and *in vivo* findings affirmed a role for ALK7 in mediating endothelial ablation during tumor invasion in PDAC.

DISCUSSION

In contrast to many tumors that are highly angiogenic, PDAC is poorly vascularized (7, 26), a paradoxical finding in light of the fact that pancreatic cancer cells are also known to express and secrete a plethora of proangiogenic factors (27). Using our 3D organotypic model to recapitulate invasion of PDAC tumor cells to blood vessels, we observed that PDAC tumor cells rapidly penetrated the lumen of blood vessels and ablated the endothelial cells, ultimately leaving lumens lined by tumor cells. We refer to this process as endothelial ablation. Furthermore, through histologic costaining of vascular basement membranes, endothelial cells, and PDAC cells within mouse tumor models, we observed that endothelial ablation by PDAC tumors occurs in the *in vivo* setting. Our study is consistent with histologic studies of PDAC patient tumors, which have reported luminal walls of arteriolar vessels that were lined by cuboidal epithelial cells in place of normal endothelium (8–10). Our study suggests that one factor contributing to the apparent microvascular hypovascularity of PDAC is not a result of reduced angiogenesis *per se*, but instead a result of endothelial ablation triggered by the invading tumor cells. These invading tumor cells exhibited a faster growth

rate than the endothelial cells and eventually led to apoptosis in tumor endothelial cells and subsequently diminished the number of functional blood vessels in the PDAC tumor microenvironment. Perhaps, our observation of tumor endothelial cell ablation in PDAC fits a classical concept of cell-cell competition, which describes clearance of “loser cells” by “winner cells” based on their fitness differences within the local environment such as their cellular division potential (28).

The ability of PDAC tumors to rapidly invade into the vessel, ablate the endothelium, and occupy the vessel lumen could explain the high rate of circulating tumor cells and metastatic load of PDAC. A similar mechanism, where tumor cells ablate the stromal cells, has been reported in a study of ovarian cancer (29). In that study, after ovarian cancer spheroids were plated on a monolayer of endometrial cells, the ovarian cancer cells began to spread over the endometrial monolayer and displaced the endometrial cells. A histologic study of ovarian cancer in human patients also reported the absence of the endometrium due to the penetration of ovarian cancer cells into the endometrium (30). In the context of these studies, our work suggests that carcinoma cells have the capacity to clear and ablate luminal compartments within the tumor microenvironment. It would be interesting to examine this phenomenon of endothelial ablation or stromal ablation in other types of cancer.

Apart from proposing a possible mechanism for the apparent hypovascularity in PDAC, our study unveils a crucial role for activin-ALK7 signaling to contribute to endothelial ablation. Although the functional roles of TGF- β and TGF- β receptor signaling have been investigated in cancer progression, little is known about the contribution of activin and ALK7 to pancreatic cancer. In ovarian cancer, hepatoma, and breast cancer, ALK7 serves as a tumor-suppressive receptor to induce apoptosis in cancer cells or prevent cancer progression (31–33). In contrast, overexpression of ALK7 has been reported to be a marker for poor prognosis in gallbladder cancer (34). ALK7 is a receptor for both nodal and activin (35). Nodal has been reported to mediate vascular mimicry in melanomas, wherein cancer cells formed perfused tubular structures and coexpressed endothelial cell markers (36). Additionally, nodal has also been found to initiate cancer stem cells in pancreatic cancer (37). In contrast, the role of activin in tumor progression has remained largely unappreciated, although activin levels in plasma have been associated with poor prognosis (38) and are overexpressed in multiple human pancreatic cancer cells (39). These reports and our findings together suggest that further investigations into the role of the activin-ALK7 axis in PDAC progression are warranted.

In this study, we use a 3D organotypic model to demonstrate that tumor-endothelial cell interactions not only are restricted to intravasation, extravasation, and vascular mimicry (36, 40) but also include the process of endothelial ablation within the blood vessels, a process that requires further study. Our simple model of PDAC and blood vessels provided sufficient complexity to reveal this process, yet allowed us to introduce genetic and spatiotemporal control to isolate signaling pathways involved for each cell type. Going forward, inclusion of vascular mural cells, and immune cells, or varying the composition of extracellular matrices could be introduced in this engineered 3D organotypic model to more faithfully study the roles of the tumor microenvironments during tumor progression *in vitro*. Although existing *in vivo* mouse models provide great opportunities to capture the progression of cancer, dissecting the molecular mechanisms and cell-cell interactions is

often difficult because of the complexity of in vivo models. Thus, as demonstrated here, 3D organotypic models provide an important complement to understand these complex cellular interactions with more mechanistic insight.

MATERIALS AND METHODS

Our device was microfabricated as previously described (18). Briefly, the polydimethylsiloxane (PDMS) device was assembled by bonding a bilayer PDMS gasket on top of a glass coverslip. Rat tail collagen 1 (Corning) was prepared at 2.5 mg/ml following the manufacturer's instructions and was injected into the PDMS device to surround two 300- μ m acupuncture needles (Hwato). After collagen polymerizes, acupuncture needles were withdrawn. HUVECs (Lonza) were seeded into one of the channels, while pancreatic cancer cells were seeded into the other channel. FBS (Atlanta Biologicals) was added at 10% (v/v) concentration into the HUVEC channel to generate a gradient of chemoattractants to trigger migration of pancreatic cancer.

Kras^{LSL-G12D}; p53^{L/+}; Pdx1-cre; Rosa26^{YFP/YFP} (KPCY) tissues were a gift from B.Z.S.'s laboratory (University of Pennsylvania). The model has been described previously (5). Briefly, mice were palpated and examined for evidence of morbidity twice per week. Tumor-bearing animals were sacrificed when morbid, and primary pancreatic tumors were collected from mice aged 14 to 30 weeks. Tissues were flash-frozen in OCT (optimal cutting temperature) and subsequently processed for immunofluorescent staining.

Detailed explanations of the materials and methods used in this study can be found in the Supplementary Materials.

SUPPLEMENTARY MATERIALS

Supplementary material for this article is available at <http://advances.sciencemag.org/cgi/content/full/5/8/eaav6789/DC1>

Fig. S1. Screening for chemoattractants for pancreatic cancer cell invasions and characterization of gradient in the 3D organotypic model.

Fig. S2. PD7591 in the biomimetic duct channel proliferated in response to the FBS gradient introduced from the biomimetic blood vessel.

Fig. S3. Vascular invasion and endothelial ablation were observed in multiple primary murine PDAC cell lines and a human pancreatic cancer cell line in our 3D biomimetic PDAC-on-a-chip model.

Fig. S4. Staining for cleaved caspase-3 and collagen IV (Col IV) in vivo and in 3D organotypic model.

Fig. S5. Tumor growth rate and caspase signal in endothelial cells in subcutaneous tumor implantation model.

Fig. S6. Inhibition of the TGF- β receptor signaling pathway reduced the endothelial ablation in human pancreatic cancer cell lines in 2D patterned coculture invasion assay and caspase staining in 2D patterned coculture.

Fig. S7. Examination of ALK4, ALK5, and ALK7 in endothelial cells and PD7591 in endothelial cell ablation.

Fig. S8. Representative images of vessel area replaced by tumor cells in 3D organotypic model.

Fig. S9. Representative images of tumor cell pattern in 2D coculture pattern assays.

Fig. S10. Schematics describing how CD31 signal intensity and cleaved caspase-3 signal intensity were measured for quantification.

Movie S1. 3D rendering of confocal image z-stack showed that YFP PD7591 (in green) invaded toward the biomimetic blood vessel (stained with CD31 in red) and wrapped around the blood vessel.

Movie S2. YFP PD7591 (in green) invaded toward the biomimetic blood vessel (stained with CD31 in red).

Movie S3. YFP PD7591 (in green) and HUVECs (in phase) were plated in 2D patterned coculture invasion assay in the presence of vehicle control (dimethyl sulfoxide).

Movie S4. YFP PD7591 (in green) and HUVECs (in phase) were plated in 2D patterned coculture invasion assay in the presence of 5 μ M SB431542.

Table S1. Oligo sequences for CRISPR.

Table S2. Primer sequences for qPCR.

Supplementary Methods

REFERENCES AND NOTES

- P. S. Steeg, Targeting metastasis. *Nat. Rev. Cancer* **16**, 201–218 (2016).
- G. P. Gupta, J. Massagué, Cancer metastasis: Building a framework. *Cell* **127**, 679–695 (2006).
- D. A. Tuveson, J. P. Neoptolemos, Understanding metastasis in pancreatic cancer: A call for new clinical approaches. *Cell* **148**, 21–23 (2012).
- A. D. Rhim, F. I. Thege, S. M. Santana, T. B. Lannin, T. N. Saha, S. Tsai, L. R. Maggs, M. L. Kochman, G. G. Ginsberg, J. G. Lieb, V. Chandrasekhara, J. A. Drebin, N. Ahmad, Y.-X. Yang, B. J. Kirby, B. Z. Stanger, Detection of circulating pancreas epithelial cells in patients with pancreatic cystic lesions. *Gastroenterology* **146**, 647–651 (2014).
- A. D. Rhim, E. T. Mirek, N. M. Aiello, A. Maitra, J. M. Bailey, F. McAllister, M. Reichert, G. L. Beatty, A. K. Rustgi, R. H. Vonderheide, S. D. Leach, B. Z. Stanger, EMT and dissemination precede pancreatic tumor formation. *Cell* **148**, 349–361 (2012).
- A. Rehders, N. H. Stoecklein, A. Güray, R. Riediger, A. Alexander, W. T. Knoefel, Vascular invasion in pancreatic cancer: Tumor biology or tumor topography? *Surgery* **152**, S143–S151 (2012).
- K. E. Craven, J. Gore, M. Korc, Overview of pre-clinical and clinical studies targeting angiogenesis in pancreatic ductal adenocarcinoma. *Cancer Lett.* **381**, 201–210 (2015).
- S.-M. Hong, M. Goggins, C. L. Wolfgang, R. D. Schulick, B. H. Edil, J. L. Cameron, A. Handra-Luca, J. M. Herman, R. H. Hruban, Vascular invasion in infiltrating ductal adenocarcinoma of the pancreas can mimic pancreatic intraepithelial neoplasia: A histopathologic study of 209 cases. *Am. J. Surg. Pathol.* **36**, 235–241 (2012).
- S. Bandyopadhyay, O. Basturk, I. Coban, D. Thirabanasak, H. Liang, D. Altinel, N. V. Adsay, Isolated solitary ducts (naked ducts) in adipose tissue: A specific but underappreciated finding of pancreatic adenocarcinoma and one of the potential reasons of understaging and high recurrence rate. *Am. J. Surg. Pathol.* **33**, 425–429 (2009).
- H. Liang, O. Basturk, S. Bandyopadhyay, D. Altinel, N. V. Adsay, Pancreatic adenocarcinoma and its mimickers: Traps in diagnosis. *Diagn. Histopathol.* **14**, 275–283 (2008).
- E. Lee, H.-H. G. Song, C. S. Chen, Biomimetic on-a-chip platforms for studying cancer metastasis. *Curr. Opin. Chem. Eng.* **11**, 20–27 (2016).
- P. Tummala, O. Junaidi, B. Agarwal, Imaging of pancreatic cancer: An overview. *J. Gastrointest. Oncol.* **2**, 168–174 (2011).
- Y. Zheng, J. Chen, M. Craven, N. W. Choi, S. Totorica, A. Diaz-Santana, P. Kermani, B. Hempstead, C. Fischbach-Teschl, J. A. López, A. D. Stroock, In vitro microvessels for the study of angiogenesis and thrombosis. *Proc. Natl. Acad. Sci. U.S.A.* **109**, 9342–9347 (2012).
- J. S. Jeon, S. Bersini, M. Gilardi, G. Dubini, J. L. Charest, M. Moretti, R. D. Kamm, Human 3D vascularized organotypic microfluidic assays to study breast cancer cell extravasation. *Proc. Natl. Acad. Sci. U.S.A.* **112**, 214–219 (2015).
- I. K. Zervantonakis, S. K. Hughes-Alford, J. L. Charest, J. S. Condeelis, F. B. Gertler, R. D. Kamm, Three-dimensional microfluidic model for tumor cell intravasation and endothelial barrier function. *Proc. Natl. Acad. Sci. U.S.A.* **109**, 13515–13520 (2012).
- H. Lee, W. Park, H. Ryu, N. L. Jeon, A microfluidic platform for quantitative analysis of cancer angiogenesis and intravasation. *Biomicrofluidics* **8**, 054102 (2014).
- M. L. Moya, Y.-H. Hsu, A. P. Lee, C. C. W. Hughes, S. C. George, In vitro perfused human capillary networks. *Tissue Eng. Part C Methods* **19**, 730–737 (2013).
- D.-H. T. Nguyen, S. C. Stapleton, M. T. Yang, S. S. Cha, C. K. Choi, P. A. Galie, C. S. Chen, Biomimetic model to reconstitute angiogenic sprouting morphogenesis in vitro. *Proc. Natl. Acad. Sci. U.S.A.* **110**, 6712–6717 (2013).
- S. M. Ehsan, K. M. Welch-Reardon, M. L. Waterman, C. C. W. Hughes, S. C. George, A three-dimensional in vitro model of tumor cell intravasation. *Integr. Biol.* **6**, 603–610 (2014).
- A. Sobrino, D. T. T. Phan, R. Datta, X. Wang, S. J. Hachey, M. Romero-Lopez, E. Gratton, A. P. Lee, S. C. George, C. C. W. Hughes, 3D microtumors in vitro supported by perfused vascular networks. *Sci. Rep.* **6**, 31589 (2016).
- M. Chung, J. Ahn, K. Son, S. Kim, N. L. Jeon, Biomimetic model of tumor microenvironment on microfluidic platform. *Adv. Healthc. Mater.* **6**, 1700196 (2017).
- C. B. Westphalen, K. P. Olive, Genetically engineered mouse models of pancreatic cancer. *Cancer J.* **18**, 502–510 (2012).
- D. Padua, J. Massagué, Roles of TGF β in metastasis. *Cell Res.* **19**, 89–102 (2009).
- G. J. Inman, F. J. Nicolás, J. F. Callahan, J. D. Harling, L. M. Gaster, A. D. Reith, N. J. Laping, C. S. Hill, SB-431542 is a potent and specific inhibitor of transforming growth factor- β superfamily type I activin receptor-like kinase (ALK) receptors ALK4, ALK5, and ALK7. *Mol. Pharmacol.* **62**, 65–74 (2002).
- A. E. Harrington, S. A. Morris-Triggs, B. T. Ruotolo, C. V. Robinson, S.-i. Ohnuma, M. Hyvönen, Structural basis for the inhibition of activin signalling by follistatin. *EMBO J.* **25**, 1035–1045 (2006).
- K. P. Olive, M. A. Jacobetz, C. J. Davidson, A. Gopinathan, D. McIntyre, D. Honess, B. Madhu, M. A. Goldgraben, M. E. Caldwell, D. Allard, K. K. Frese, G. Denicola, C. Feig, C. Combs, S. P. Winter, H. Ireland-Zecchini, S. Reichelt, W. J. Howat, A. Chang, M. Dhara, L. Wang, F. Ruckert, R. Grutzmann, C. Pilarsky, K. Izeradjene, S. R. Hingorani, P. Huang, S. E. Davies, W. Plunkett, M. Egorin, R. H. Hruban, N. Whitebread, K. McGovern, J. Adams, C. Iacobuzio-Donahue, J. Griffiths, D. A. Tuveson, Inhibition of Hedgehog signaling enhances delivery of chemotherapy in a mouse model of pancreatic cancer. *Science* **324**, 1457–1461 (2009).
- M. Korc, Pathways for aberrant angiogenesis in pancreatic cancer. *Mol. Cancer* **2**, 8 (2003).

28. R. Gogna, K. Shee, E. Moreno, Cell competition during growth and regeneration. *Annu. Rev. Genet.* **49**, 697–718 (2015).
29. R. A. Davidowitz, L. M. Selfors, M. P. Iwanicki, K. M. Elias, A. Karst, H. Piao, T. A. Ince, M. G. Drage, J. Dering, G. E. Konecny, U. Matulonis, G. B. Mills, D. J. Slamon, R. Drapkin, J. S. Brugge, Mesenchymal gene program-expressing ovarian cancer spheroids exhibit enhanced mesothelial clearance. *J. Clin. Invest.* **124**, 2611–2625 (2014).
30. C. A. Witz, I. A. Monotoya-Rodriguez, R. S. Schenken, Whole explants of peritoneum and endometrium: A novel model of the early endometriosis lesion. *Fertil. Steril.* **71**, 56–60 (1999).
31. G. Xu, H. Zhou, Q. Wang, N. Auersperg, C. Peng, Activin receptor-like kinase 7 induces apoptosis through up-regulation of Bax and down-regulation of Xiap in normal and malignant ovarian epithelial cell lines. *Mol. Cancer Res.* **4**, 235–246 (2006).
32. B.-C. Kim, H. van Gelder, T. A. Kim, H.-J. Lee, K. G. Baik, H. H. Chun, D. A. Lee, K. S. Choi, S.-J. Kim, Activin receptor-like kinase-7 induces apoptosis through activation of MAPKs in a Smad3-dependent mechanism in hepatoma cells. *J. Biol. Chem.* **279**, 28458–28465 (2004).
33. F. Zeng, G. Xu, T. Zhou, C. Yang, X. Wang, C. Peng, H. Zhou, Reduced expression of activin receptor-like kinase 7 in breast cancer is associated with tumor progression. *Med. Oncol.* **29**, 2519–2526 (2012).
34. J. Li, Z. Yang, Q. Zou, Y. Yuan, J. Li, L. Liang, G. Zeng, S. Chen, PKM2 and ACVR 1C are prognostic markers for poor prognosis of gallbladder cancer. *Clin. Transl. Oncol.* **16**, 200–207 (2014).
35. L. M. Wakefield, C. S. Hill, Beyond TGF β : Roles of other TGF β superfamily members in cancer. *Nat. Rev. Cancer* **13**, 328–341 (2013).
36. L.-M. Postovit, N. V. Margaryan, E. A. Seftor, M. J. C. Hendrix, Role of nodal signaling and the microenvironment underlying melanoma plasticity. *Pigment Cell Melanoma Res.* **21**, 348–357 (2008).
37. E. Lonardo, P. C. Hermann, M. T. Mueller, S. Huber, A. Balic, I. Miranda-Lorenzo, S. Zagorac, S. Alcalá, I. Rodriguez-Arabaolaza, J. C. Ramirez, R. Torres-Ruiz, E. Garcia, M. Hidalgo, D. A. Cebrián, R. Heuchel, M. Löhr, F. Berger, P. Bartenstein, A. Aicher, C. Heeschen, Nodal/Activin signaling drives self-renewal and tumorigenicity of pancreatic cancer stem cells and provides a target for combined drug therapy. *Cell Stem Cell* **9**, 433–446 (2011).
38. Y. Togashi, A. Kogita, H. Sakamoto, H. Hayashi, M. Terashima, M. A. de Velasco, K. Sakai, Y. Fujita, S. Tomida, M. Kitano, K. Okuno, M. Kudo, K. Nishio, Activin signal promotes cancer progression and is involved in cachexia in a subset of pancreatic cancer. *Cancer Lett.* **356**, 819–827 (2015).
39. J. Kleeff, T. Ishiwata, H. Friess, M. W. Buchler, M. Korc, Concomitant over-expression of activin/inhibin β subunits and their receptors in human pancreatic cancer. *Int. J. Cancer* **77**, 860–868 (1998).
40. N. Reymond, B. B. d'Água, A. J. Ridley, Crossing the endothelial barrier during metastasis. *Nat. Rev. Cancer* **13**, 858–870 (2013).

Acknowledgments: We wish to thank A. Rhim, N. Aiello, S. Yuan, and B. Bakir for providing cell lines and advice. We thank J. Yang for technical assistance and T. Mirabella for helpful discussions. **Funding:** This work was supported, in part, by grants from the NIH (EB00262, UH3EB017103, and UC4DK104196). E.L. acknowledges financial support from a LE&RN postdoctoral grant from Lymphatic Education and Research Network and a BU-CTSI grant (TL1TR001410) from the National Center for Advancing Translational Sciences at the NIH. J.J.-K.L. acknowledges financial support from the Harvard Ludwig Center. **Author contributions:** D.-H.T.N. and E.L. designed and performed experiments. S.A., R.J.N., A.W., J.J.-K.L., and J.E. performed the experiments and data analysis. D.-H.T.N., E.L., J.E., B.Z.S., and C.S.C. wrote the manuscript. B.Z.S. and C.S.C. supervised the project. **Competing interests:** The authors declare that they have no competing interests. **Data and materials availability:** All data needed to evaluate the conclusions in the paper are present in the paper and/or the Supplementary Materials. Additional data related to this paper may be requested from the authors.

Submitted 10 October 2018

Accepted 25 July 2019

Published 28 August 2019

10.1126/sciadv.aav6789

Citation: D.-H. T. Nguyen, E. Lee, S. Alimperti, R. J. Norgard, A. Wong, J. J.-K. Lee, J. Eyckmans, B. Z. Stanger, C. S. Chen, A biomimetic pancreatic cancer on-chip reveals endothelial ablation via ALK7 signaling. *Sci. Adv.* **5**, eaav6789 (2019).

A biomimetic pancreatic cancer on-chip reveals endothelial ablation via ALK7 signaling

Duc-Huy T. Nguyen, Esak Lee, Styliani Alimperti, Robert J. Norgard, Alec Wong, Jake June-Koo Lee, Jeroen Eyckmans, Ben Z. Stanger and Christopher S. Chen

Sci Adv 5 (8), eaav6789.
DOI: 10.1126/sciadv.aav6789

| | |
|-------------------------|---|
| ARTICLE TOOLS | http://advances.sciencemag.org/content/5/8/eaav6789 |
| SUPPLEMENTARY MATERIALS | http://advances.sciencemag.org/content/suppl/2019/08/26/5.8.eaav6789.DC1 |
| REFERENCES | This article cites 40 articles, 9 of which you can access for free http://advances.sciencemag.org/content/5/8/eaav6789#BIBL |
| PERMISSIONS | http://www.sciencemag.org/help/reprints-and-permissions |

Use of this article is subject to the [Terms of Service](#)

Science Advances (ISSN 2375-2548) is published by the American Association for the Advancement of Science, 1200 New York Avenue NW, Washington, DC 20005. 2017 © The Authors, some rights reserved; exclusive licensee American Association for the Advancement of Science. No claim to original U.S. Government Works. The title *Science Advances* is a registered trademark of AAAS.

Supplementary Materials for

A biomimetic pancreatic cancer on-chip reveals endothelial ablation via ALK7 signaling

Duc-Huy T. Nguyen, Esak Lee, Styliani Alimperti, Robert J. Norgard, Alec Wong, Jake June-Koo Lee, Jeroen Eyckmans, Ben Z. Stanger, Christopher S. Chen*

*Corresponding author. Email: chencs@bu.edu

Published 28 August 2019, *Sci. Adv.* **5**, eaav6789 (2019)
DOI: 10.1126/sciadv.aav6789

The PDF file includes:

Fig. S1. Screening for chemoattractants for pancreatic cancer cell invasions and characterization of gradient in the 3D organotypic model.

Fig. S2. PD7591 in the biomimetic duct channel proliferated in response to the FBS gradient introduced from the biomimetic blood vessel.

Fig. S3. Vascular invasion and endothelial ablation were observed in multiple primary murine PDAC cell lines and a human pancreatic cancer cell line in our 3D biomimetic PDAC-on-a-chip model.

Fig. S4. Staining for cleaved caspase-3 and collagen IV (Col IV) in vivo and in 3D organotypic model.

Fig. S5. Tumor growth rate and caspase signal in endothelial cells in subcutaneous tumor implantation model.

Fig. S6. Inhibition of the TGF- β receptor signaling pathway reduced the endothelial ablation in human pancreatic cancer cell lines in 2D patterned coculture invasion assay and caspase staining in 2D patterned coculture.

Fig. S7. Examination of ALK4, ALK5, and ALK7 in endothelial cells and PD7591 in endothelial cell ablation.

Fig. S8. Representative images of vessel area replaced by tumor cells in 3D organotypic model.

Fig. S9. Representative images of tumor cell pattern in 2D coculture pattern assays.

Fig. S10. Schematics describing how CD31 signal intensity and cleaved caspase-3 signal intensity were measured for quantification.

Legends for movies S1 to S4

Table S1. Oligo sequences for CRISPR.

Table S2. Primer sequences for qPCR.

Supplementary Methods

Other Supplementary Material for this manuscript includes the following:

(available at advances.sciencemag.org/cgi/content/full/5/8/eaav6789/DC1)

Movie S1 (.mov format). 3D rendering of confocal image z-stack showed that YFP PD7591 (in green) invaded toward the biomimetic blood vessel (stained with CD31 in red) and wrapped around the blood vessel.

Movie S2 (.avi format). YFP PD7591 (in green) invaded toward the biomimetic blood vessel (stained with CD31 in red).

Movie S3 (.avi format). YFP PD7591 (in green) and HUVECs (in phase) were plated in 2D patterned coculture invasion assay in the presence of vehicle control (dimethyl sulfoxide).

Movie S4 (.avi format). YFP PD7591 (in green) and HUVECs (in phase) were plated in 2D patterned coculture invasion assay in the presence of 5 μ M SB431542.

Supplementary Materials

Supplementary Figures and Legends:

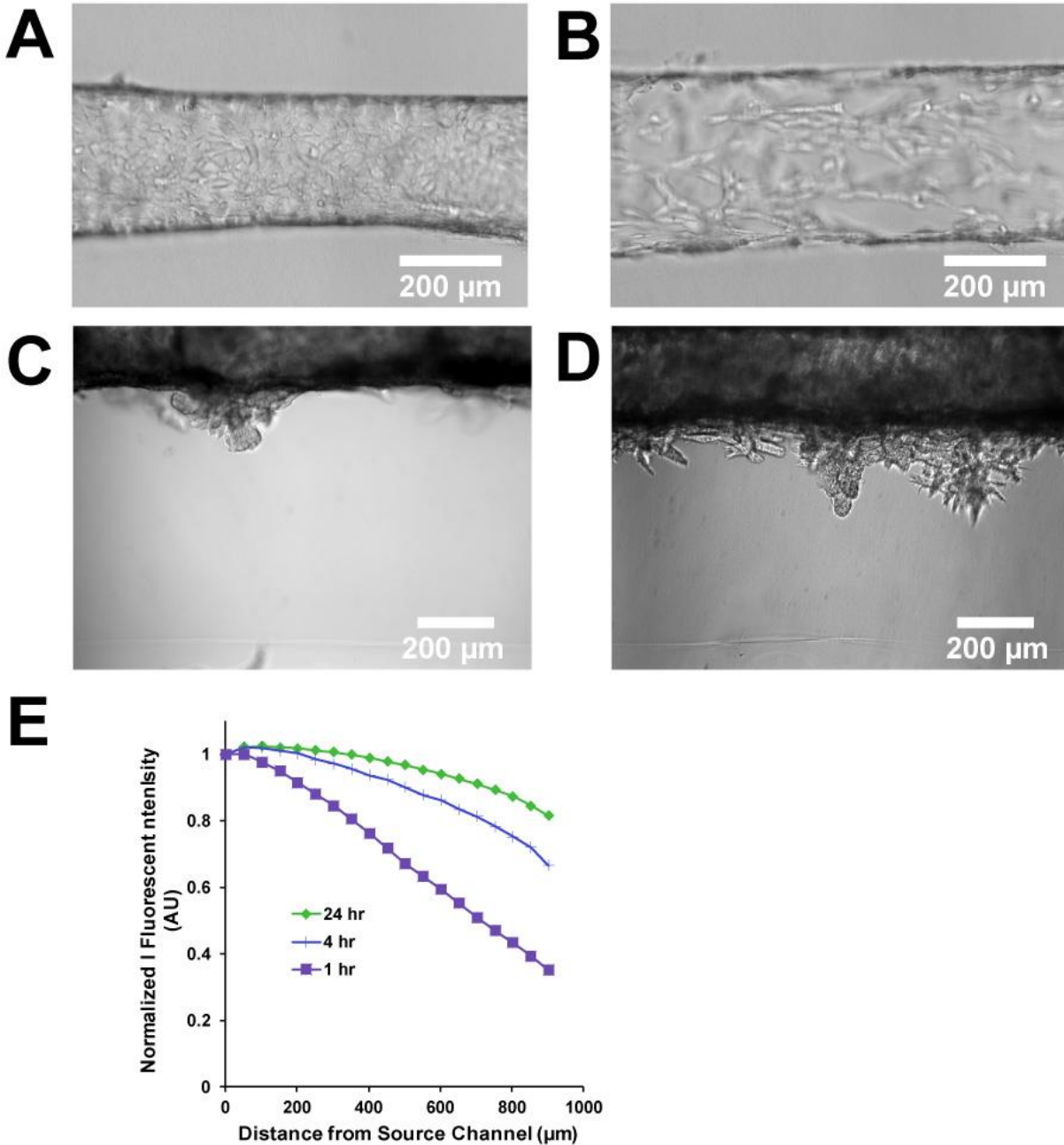


Fig. S1. Screening for chemoattractants for pancreatic cancer cell invasions and characterization of gradient in the 3D organotypic model. The two channels were 1mm apart. (A) PDAC seeded at Day 0 in the channel in endothelial cell basal medium (EBM2). The source channel without endothelial cells is

endothelial cell basal medium supplemented with the following factors: 100ng/ml MCP1, 100ng/ml HGF, 100ng/ml EGF, 100ng/ml VEGF, 100ng/ml bFGF, and 100ng/ml SDF1 α . **(B)** The same device at Day 3 where PDAC was seeded and exposed to the combination of several factors in A). The PDAC failed to survive or invade and the remaining cells scarcely occupied the channel. **(C)** PDAC invasion in response to 10% FBS in the device at Day 9. **(D)** PDAC invasion in response to 20% FBS in the device at Day 9. PDAC migrated towards the source channel more robustly with multiple locations on the channel exhibiting protrusive activities. **(E)** Characterization of the gradient in the device whose two channels were 1mm apart. 21kDa fluorescein isothiocyanate (FITC-dextran) dextran fluorescent was introduced into one channel. The signal intensity of dextran was imaged along the distance between the two channels at 1, 4, and 24hrs. Gradient was established at 1hr. A shallow gradient was still maintained at 24hr.

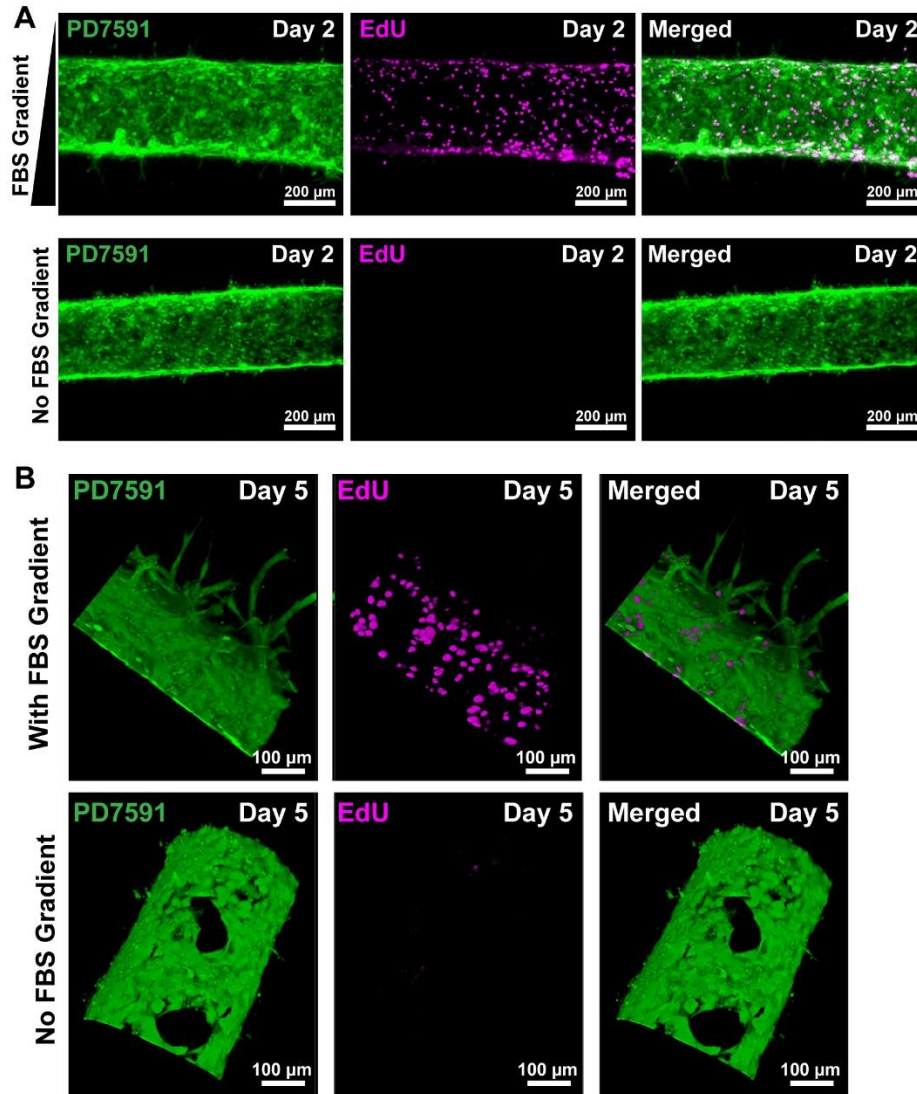


Fig. S2. PD7591 in the biomimetic duct channel proliferated in response to the FBS gradient introduced from the biomimetic blood vessel. (A) EdU staining at Day 2 when FBS was added into the biomimetic blood vessel vs when FBS was not added into the biomimetic blood vessel. PD7591 proliferated when exposed to the FBS gradient but exhibited minimal proliferation without the addition of FBS in the biomimetic blood vessel. **(B)** EdU staining at Day 5 when FBS was added into the biomimetic blood vessel vs when FBS was not present in the biomimetic blood vessel. PD7591 proliferated in the biomimetic duct channel in the presence of FBS gradient and multiple invasive cells toward the FBS gradient were also stained positive for EdU.

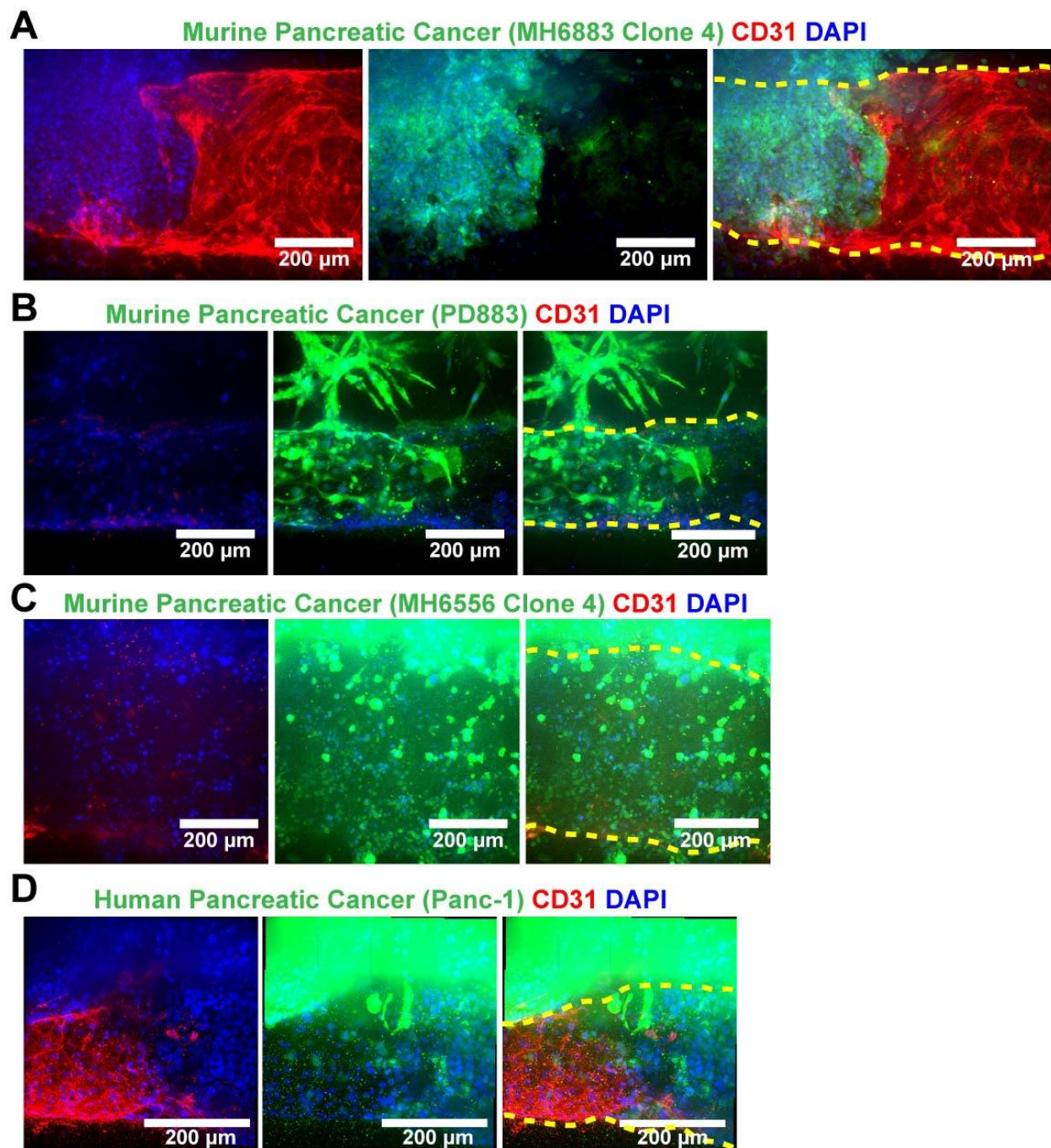


Fig. S3. Vascular invasion and endothelial ablation were observed in multiple primary murine PDAC cell lines and a human pancreatic cancer cell line in our 3D biomimetic PDAC-on-a-chip model. We observed vascular invasion and endothelial ablation by murine primary pancreatic cancer cell lines: **(A)** MH6883, Clone 4, **(B)** PD883, and **(C)** MH6556, Clone 4; and by the human pancreatic cancer cell line **(D)** Panc-1. In all images, pancreatic cancer cells were re-stained with FITC-conjugated anti-GFP antibody (in green). HUVECs were stained with CD31 (in red), and cell nuclei were stained with DAPI (in blue). Blood vessels were delineated by yellow dash lines.

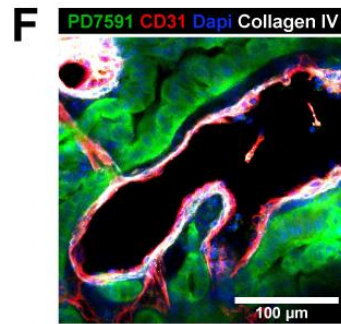
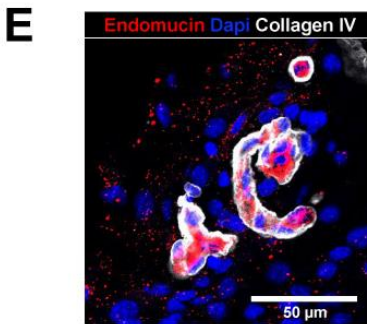
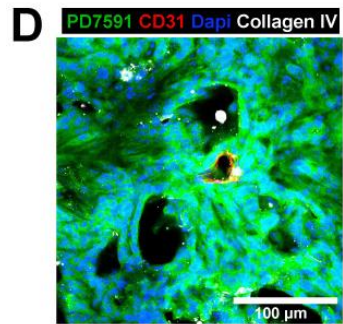
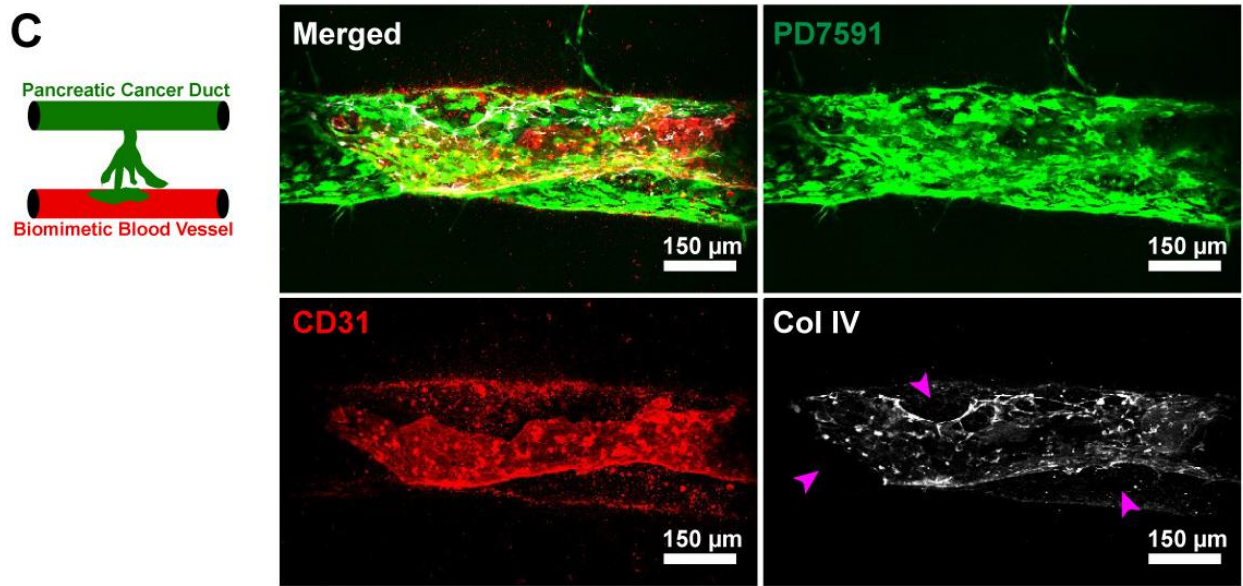
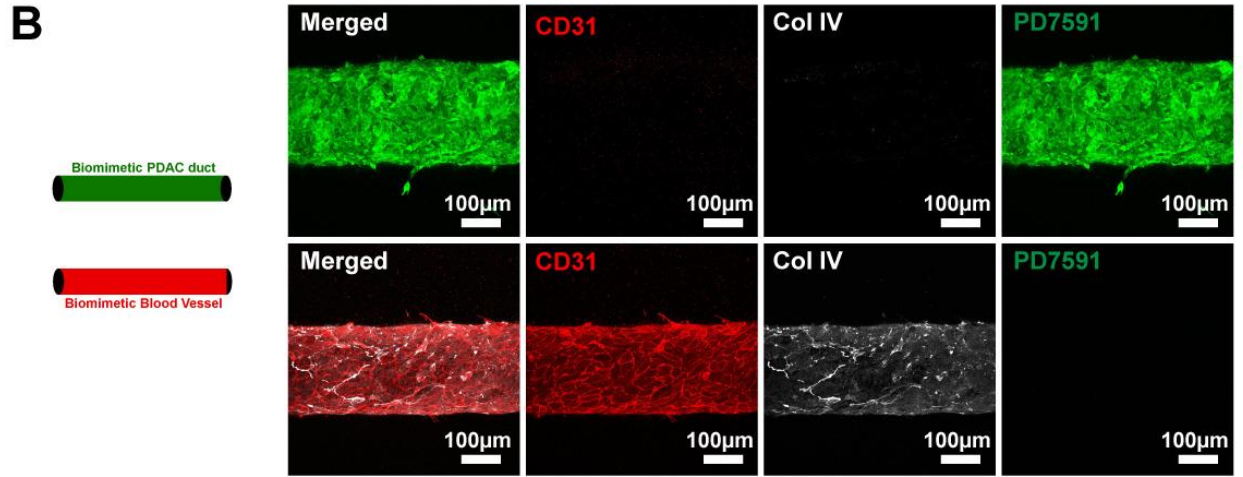
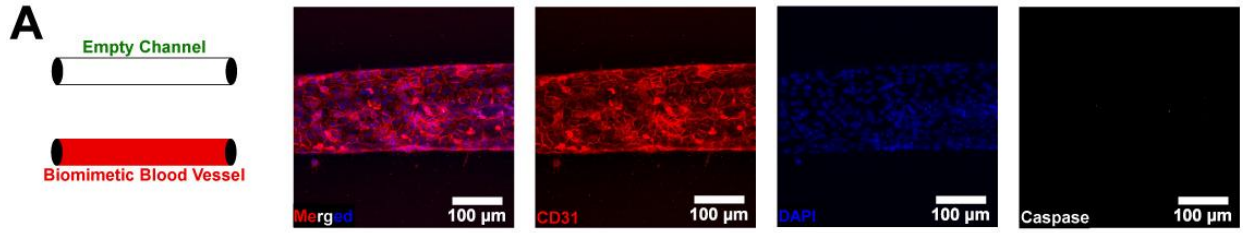


Fig. S4. Staining for cleaved caspase-3 and collagen IV (Col IV) in vivo and in 3D organotypic

model. (A) Biomimetic blood vessel displays no apoptotic cleaved caspase-3 signal without tumor cell invasion. Endothelial cells were stained with CD31 (red), DAPI (blue), and cleaved caspase-3 (white). **(B)** Deposition of collagen IV by endothelial cells was present in our 3D biomimetic blood vessel. PD7591 deposited no collagen IV upon seeding into the pancreatic duct. **(C)** As tumor cells invaded into the biomimetic blood vessel, the layer of collagen IV gradually disappeared (pink arrows showed areas where collagen IV disappeared). **(D)** PD7591 deposited no collagen IV when subcutaneously injected into the mice. **(E)** Collagen IV (white) was strongly present in blood vessels (stained by Endomucin in red) in an adjacent tissue without any tumor invasion in our *in vivo* tumor implantation mice model. **(F)** A section of tumor in subcutaneous implantation mouse model showed that the collagen IV in basement membrane remained intact when tumor cells didn't invade into the vessel. HUVECs were stained with CD31 (in red), cell nuclei were stained with DAPI (in blue), PD7591 was stained with anti-GFP (in green), and collagen IV was stained with anti-collagen IV (in white).

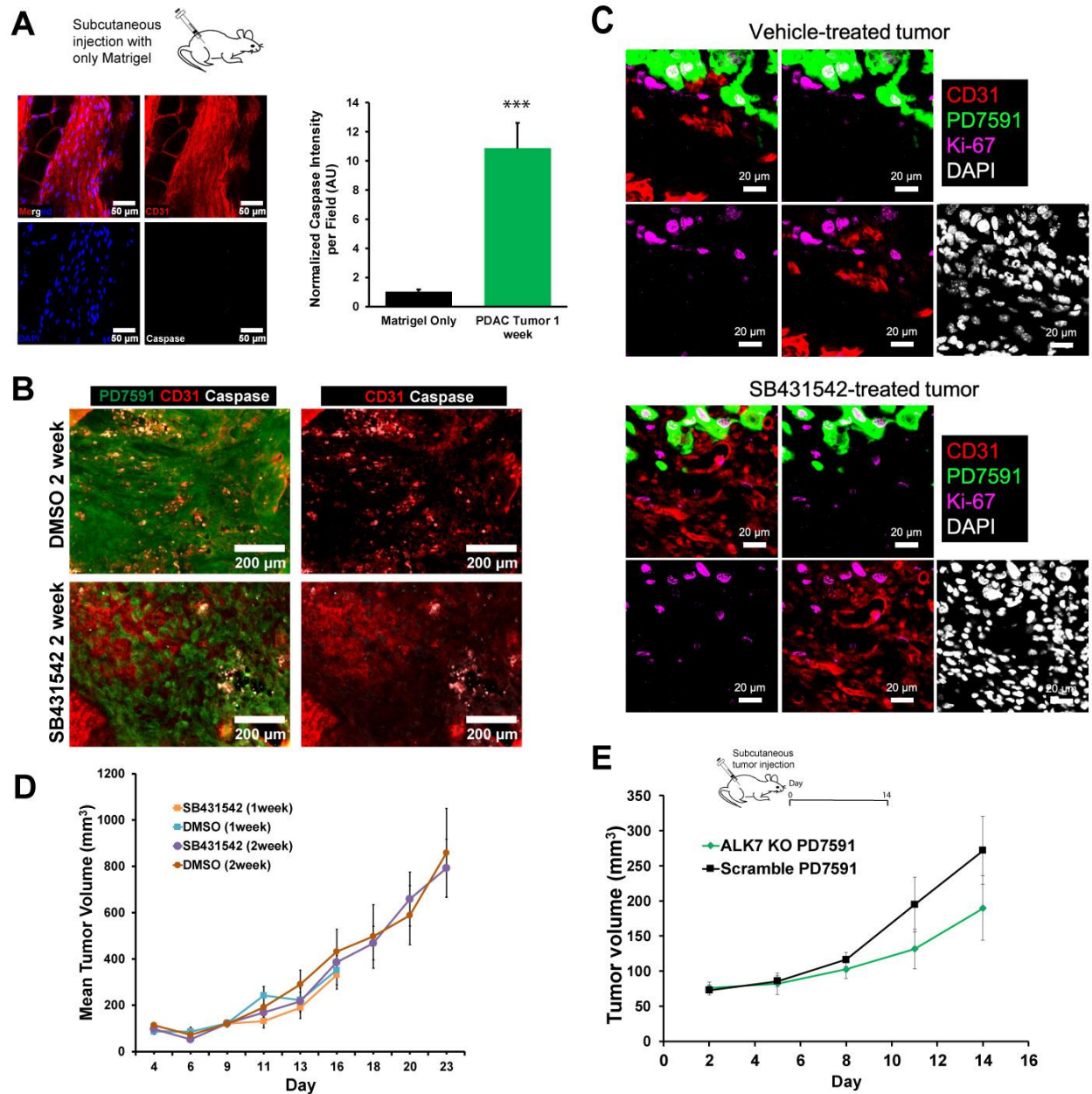


Fig. S5. Tumor growth rate and caspase signal in endothelial cells in subcutaneous tumor implantation model. (A) Mice were implanted with Matrigel only (without tumor cells). We also quantified the signal intensity in cleaved caspase-3 in endothelial cells for mice injected with Matrigel only for 1 week vs mice injected with Matrigel and tumor cells for 1 week. The tissue with tumor implanted significantly displayed higher caspase signal intensity as compared to tissue with Matrigel only ($n=3$ mice/group and a total of 10 tissue sections were examined per group of mice). (B) Representative images of tumor tissue sections stained with CD31 (red) and cleaved caspase-3 (white) for mice treated

with DMSO and SB431542 for 2 weeks. PD7591 was co-stained with anti-GFP (in green). **(C)** Ki-67 staining in tumor tissue. Ki-67 was stained for mice treated with DMSO and SB431542 for 1 week. We observed the majority of endothelial cells in tissues were negative for Ki-67, suggesting very minimal angiogenesis in tumors treated with DMSO and SB431542. **(D)** Tumor growth rate for different groups of mice: DMSO treated mice for 1 week, SB431542 treated mice for 1 week, DMSO treated mice for 2 weeks, and SB431542 treated mice for 2 weeks. SB431542 didn't alter the tumor growth rate as compared to DMSO control groups for both 1-week and 2-week treatments. **(E)** Tumor growth in mice implanted with ALK7 KO vs Scramble tumor cells. PD7591 tumor cells were either transduced with Crispr-mediated knockout ALK7 lentiviruses or Scramble lentiviruses. Two million of ALK7 KO PD7591 or Scramble PD7591 cells were subcutaneously implanted into mice (n=5 mice/group). After two weeks, mice were sacrificed, and tumors were harvested. Mice with ALK7 KO PD7591 displayed a delay in tumor growth as compared to mice with Scramble PD7591.

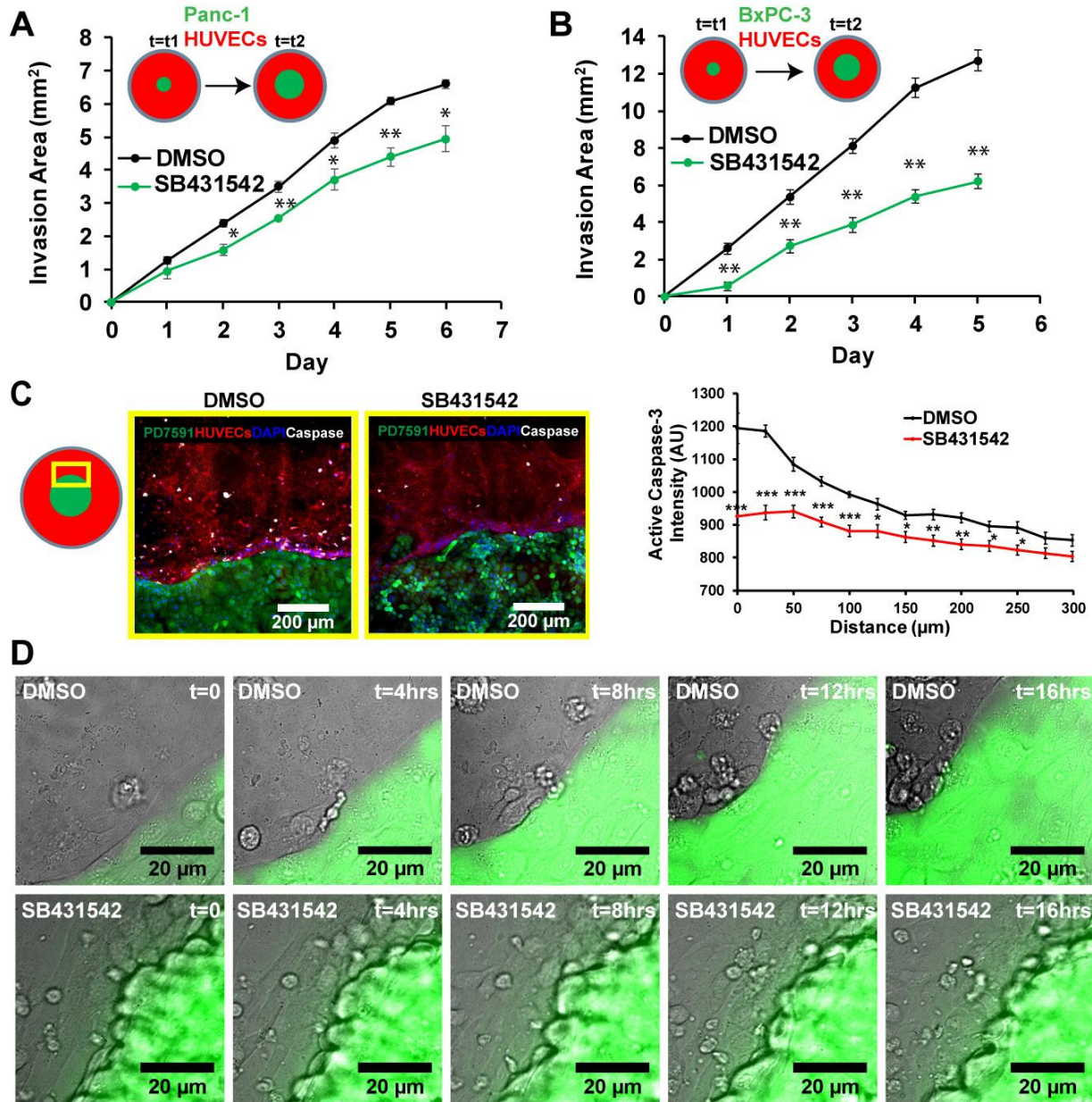


Fig. S6. Inhibition of the TGF- β receptor signaling pathway reduced the endothelial ablation in human pancreatic cancer cell lines in 2D patterned coculture invasion assay and caspase staining in 2D patterned coculture. (A) A human pancreatic cancer cell line Panc-1 and HUVECs were patterned in 2D cocultures with DMSO or 5 μ M SB431542. SB431542 effectively reduced endothelial ablation by Panc-1 cells (n=3 individual experiments). (B) A human pancreatic cancer cell line BxPC-3 and HUVECs were patterned in 2D cocultures with DMSO or 5 μ M SB431542. SB431542 significantly delayed endothelial ablation by Panc-1 cells or BxPC-3 cells (n=3 individual experiments). (C) Inhibition of TGF- β

receptor signaling pathway reduced the endothelial ablation and apoptosis in endothelial cells in 2D patterned coculture invasion assay. Cleaved caspase-3 (in white) was stained and quantified. The cleaved caspase-3 signal intensity was reported as a function of distance away from the boundary between tumor cell PD7591 (green) and endothelial cells (red). The cleaved caspase-3 signal was localized mostly at the endothelial cells in proximity to the tumor cells and significantly dropped as the endothelial cells were farther way from the tumor cells. Inhibition of TGF- β receptor signaling pathway significantly reduced the cleaved caspase-3 signal intensity (n=5 patterns from 5 individual experiments).

(D) Snap shot images of time lapse movies where tumor cells PD7591 invaded into the monolayer of endothelial cells in 2D patterned coculture assay. At t=8hr, there were more endothelial cells that appeared to round up and detached from the surface, which resembled behavior of cells undergoing apoptosis. Inhibition of TGF- β receptor signaling pathway reduced and delayed the appearance of round and detached endothelial cells at the interface between tumor cells and endothelial cells.* (p<0.05) and ** (p<0.01) indicate statistical significance. Two-tailed Student's t-test. Error bars are SEM.

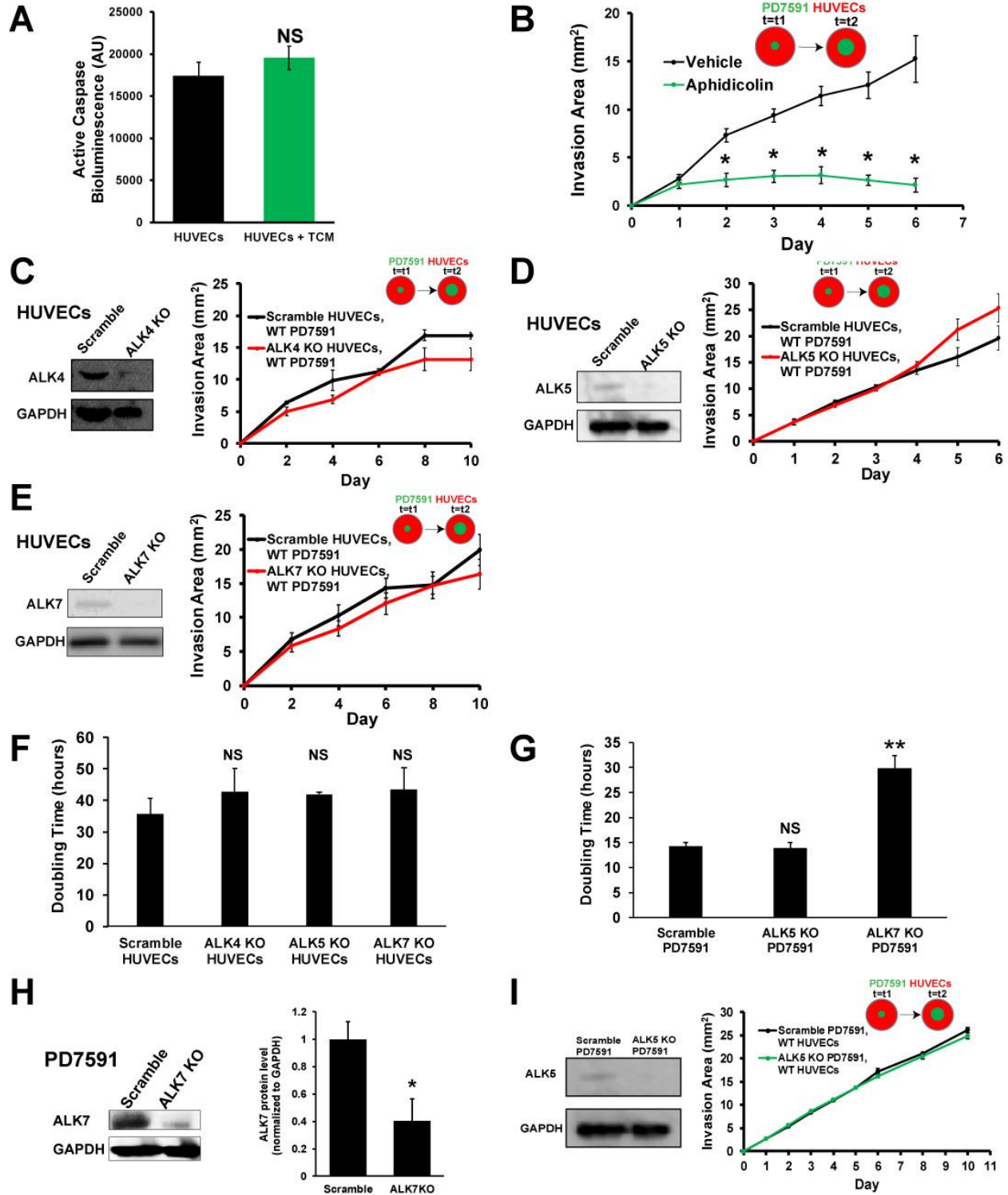


Fig. S7. Examination of ALK4, ALK5, and ALK7 in endothelial cells and PD7591 in endothelial cell ablation. (A) Conditioned medium was collected from tumor cells and added into a monolayer of endothelial cells. No significant difference in active caspase bioluminescent signal between conditioned

medium vs control condition (n=3 individual experiments). **(B)** Inhibition of proliferation with aphidicolin (0.5µg/ml) in 2D coculture pattern assay showed that inhibition of proliferation significantly reduced endothelial cell ablation, suggesting an important role of tumor cell proliferation in endothelial cell ablation (n=3 individual experiments). **(C)** Knock out of ALK4 in endothelial cells did not significantly reduce endothelial ablation (n=3 individual experiments). Western blot indicated efficient knock out of ALK4 in endothelial cells with CRISPR/Cas9 technology. **(D)** Knock out of ALK5 in endothelial cells did not significantly reduce endothelial ablation (n=3 individual experiments). Western blot indicated efficient knock out of ALK5 in endothelial cells with CRISPR/Cas9 technology. **(E)** Knock out of ALK7 in endothelial cells did not significantly reduce endothelial ablation (n=3 individual experiments). Western blot indicated efficient knock out of ALK7 in endothelial cells with CRISPR/Cas9 technology. **(F)** Doubling times of HUVECs when ALK4, 5, 7 receptors were knocked out in comparison to control Scramble HUVECs. There was no significant difference in proliferation when each of these receptors was knocked out in HUVECs (n=3 individual experiments). **(G)** Doubling times of PD7591 when ALK5, and 7 receptors were knocked out in comparison to control Scramble PD7591. Only when ALK7 receptor was knocked out, the doubling time of PD7591 was significantly higher than in Scramble control PD7591 (n=3 individual experiments). **(H)** Western blot of ALK7 knocked out PD7591 cells showed a reduction in the ALK7 protein level in PD7591 (n=3 individual experiments). **(I)** Western blot indicated the efficient knockout of ALK5 in PD7591. However, ALK5 knockout PD7591 did not affect endothelial ablation as shown in 2D patterned coculture (n=3 individual experiments). * (p<0.05) indicates statistical significance. NS indicates non-statistical significance. Two-tailed Student's t-test. Error bars are SEM.

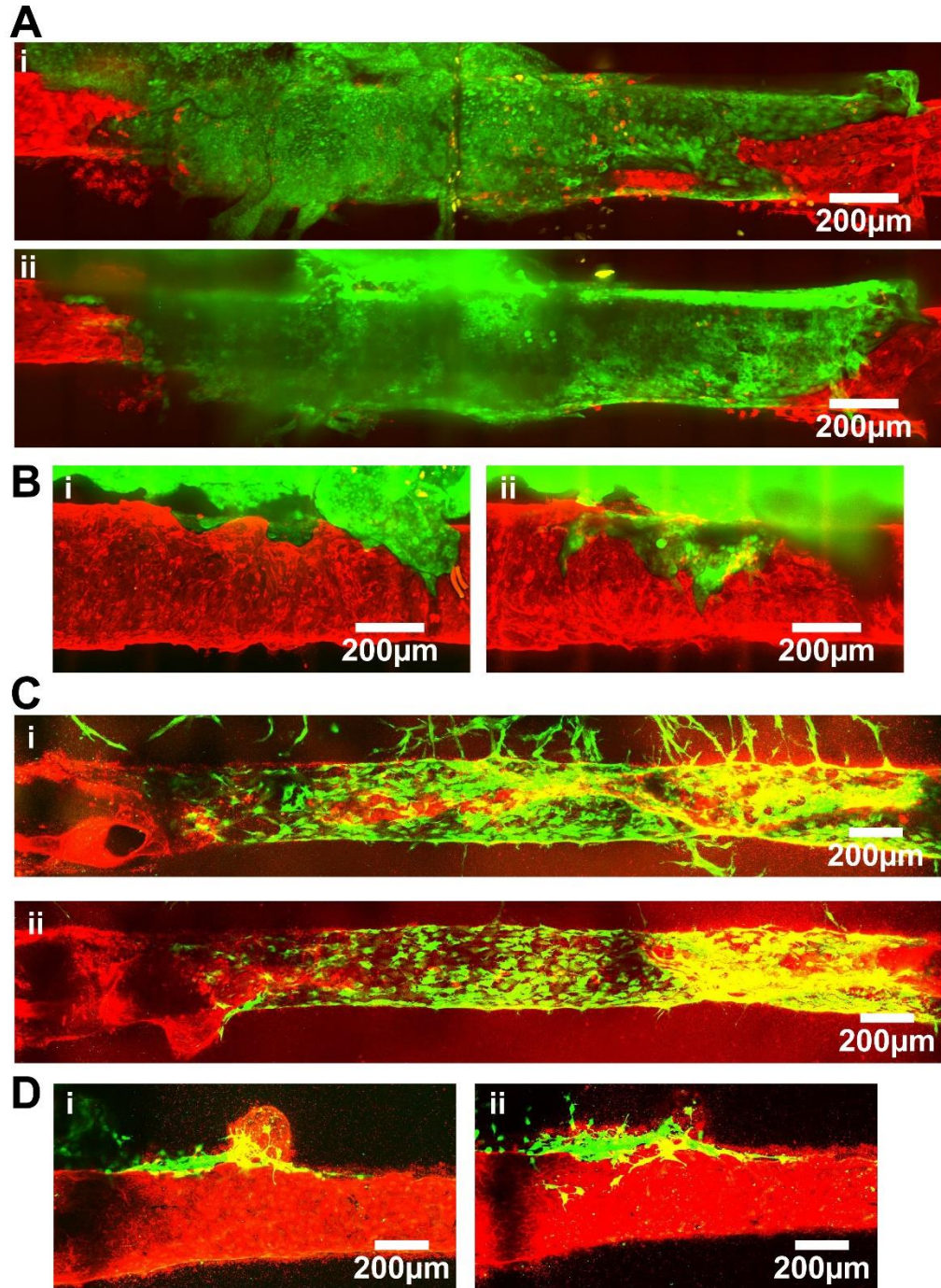


Fig. S8. Representative images of vessel area replaced by tumor cells in 3D organotypic model.

Representative images of vessel area replaced by tumor cells in 3D organotypic model for experiment with SB431542 (A and B), and follistatin (C and D). Endothelial cells were stained with CD31 (in red) and tumor PD7591 was stained with anti-GFP (in green). (A) Representative images for control device treated with DMSO for experiment with SB431542. (i) Z projection of the bottom half of the biomimetic vessel. (ii)

Z projection of the top half of the biomimetic vessel. **(B)** Representative images for device treated with 5 μ M SB431542. (i) Z projection of the bottom half of the biomimetic vessel. (ii) Z projection of the top half of the biomimetic vessel. **(C)** Representative images for control device for experiment with follistatin. (i) Z projection of the bottom half of the biomimetic vessel. (ii) Z projection of the top half of the biomimetic vessel. **(D)** Representative images for device treated with 200ng/ml follistatin for experiment with follistatin. (i) Z projection of the bottom half of the biomimetic vessel. (ii) Z projection of the top half of the biomimetic vessel.

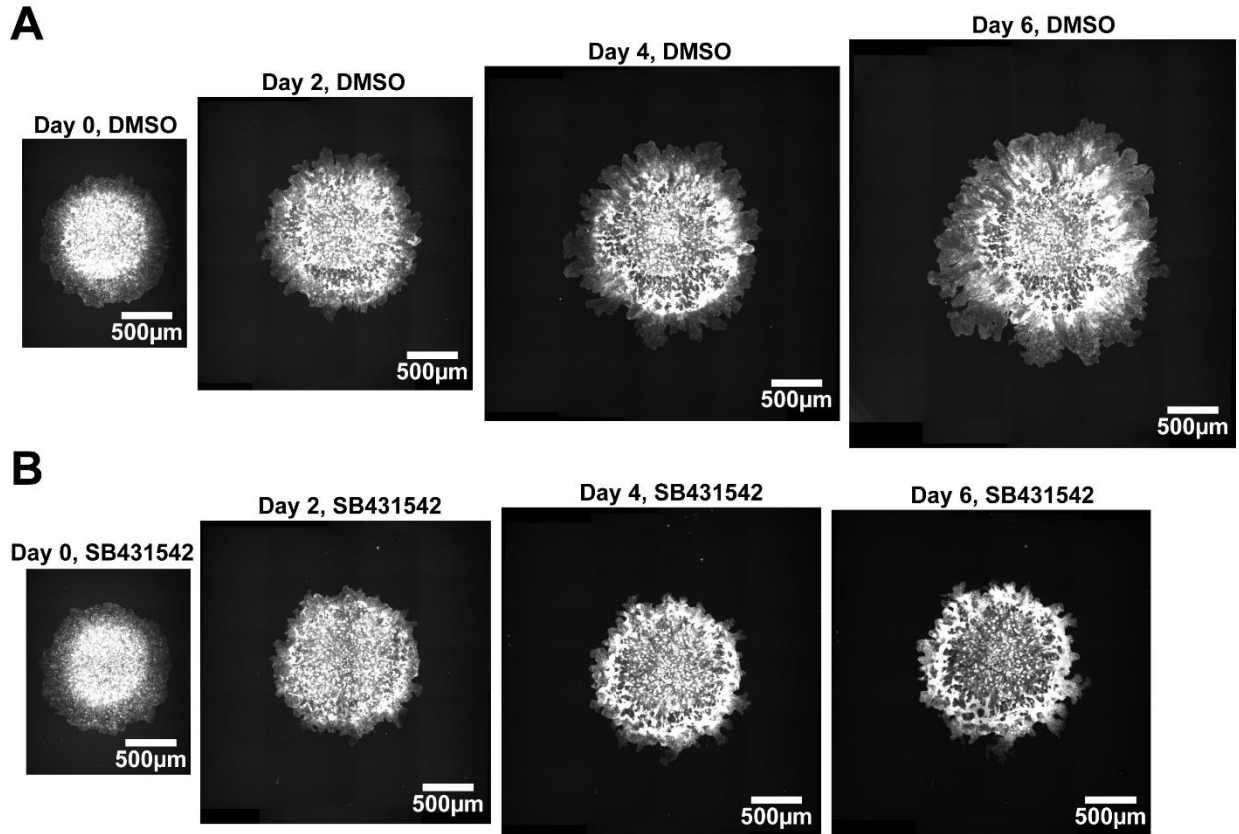


Fig. S9. Representative images of tumor cell pattern in 2D coculture pattern assays. (A)

Representative images of the whole tumor cell pattern in control DMSO condition over time. The whole tumor cell pattern was acquired by stitching multiple overlapped images of YFP PD7591. **(B)**

Representative images of the whole tumor cell pattern in 5µM SB431542 condition over time. The whole tumor cell pattern was acquired by stitching multiple overlapped images of YFP PD7591.

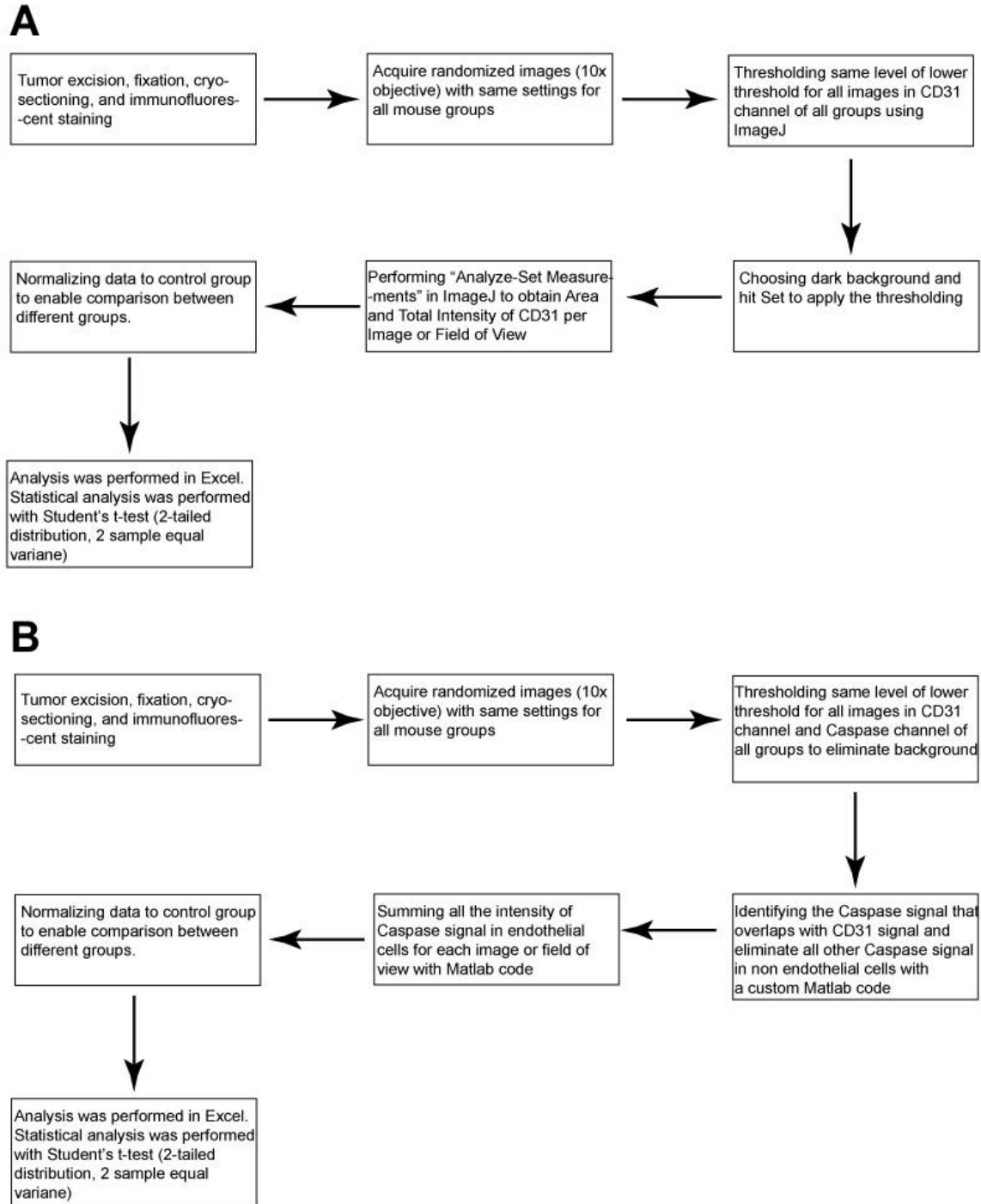


Fig. S10. Schematics describing how CD31 signal intensity and cleaved caspase-3 signal intensity were measured for quantification. (A) Schematic describing the procedure used to quantify CD31 signal intensity. **(B)** Schematic describing the procedure used to quantify cleaved caspase-3 signal intensity.

Supplementary Movie Legends:

Movie S1. 3D rendering of confocal image z-stack showed that YFP PD7591 (in green) invaded toward the biomimetic blood vessel (stained with CD31 in red) and wrapped around the blood vessel. Cell nuclei were stained with DAPI (in blue).

Movie S2. YFP PD7591 (in green) invaded toward the biomimetic blood vessel (stained with CD31 in red). Confocal imaging revealed that part of the vessel lumen was ablated and occupied by YFP PD7591. Cell nuclei were stained with DAPI (in blue).

Movie S3. YFP PD7591 (in green) and HUVECs (in phase) were plated in 2D patterned coculture invasion assay in the presence of vehicle control (dimethyl sulfoxide). Timelapse movie showed that YFP PD7591 (in green) invaded into a monolayer of HUVECs, and ablated the HUVECs, causing the juxtaposed HUVECs to round up. Time lapse was captured at 15 min intervals for a duration of 16 hours.

Movie S4. YFP PD7591 (in green) and HUVECs (in phase) were plated in 2D patterned coculture invasion assay in the presence of 5 μ M SB431542. Timelapse movie showed that SB431542 halted YFP PD7591 (in green) from invading into a monolayer of HUVECs, and prevented ablation of juxtaposed endothelial cells. Time lapse was captured at 15 min intervals for a duration of 16 hours.

Supplementary Tables:

Table S1. Oligo sequences for CRISPR.

| gRNA oligos (5'-3') | |
|---------------------|-----------------------------------|
| Human ALK4 oligos | <i>CACCGACCCGCCGCTGCCGGCGAGC</i> |
| | <i>AAACGCTCGCCGGCAGCGGGGGTC</i> |
| Human ALK5 oligos | <i>CACCGCATACAAACGGCCTATCTCG</i> |
| | <i>AAACCGAGATAGGCCGTTTGTATGC</i> |
| Human ALK7 oligos | <i>CACCGTGTGAAGCAGCATTTCGGTTT</i> |
| | <i>AAACAAACCGAATGCTGCTTCACAC</i> |
| Mouse ALK5 oligos | <i>CACCGTCCGCAGCTCCTCATCGTGT</i> |
| | <i>AAACACACGATGAGGAGCTGCGGAC</i> |
| Mouse ALK7 oligos | <i>CACCGCGGTTTGGGGAAGTGTGGCA</i> |
| | <i>AAACTGCCACACTTCCCCAAACCGC</i> |
| Scrambled oligos | <i>CACCGGCACTACCAGAGCTAACTCA</i> |
| | <i>AAACTGAGTTAGCTCTGGTAGTGCC</i> |

Table S2. Primer sequences for qPCR.

| Primers (5'-3') | |
|-------------------------|--------------------------------------|
| Mouse inhibin β A | <i>Forward: CTGCTGGACCAGGGAAGAG</i> |
| | <i>Reverse: AAGCACTAGACTGGCACCAC</i> |
| Mouse inhibin β B | <i>Forward: AGGAGGAAGGTACGGGTCAA</i> |
| | <i>Reverse: GTCTCTCCCCTCGCTCAAAC</i> |

Supplementary Methods

Cell culture. Primary murine pancreatic cancer cell lines YFP PD7591, YFP PD883, YFP MH6883 Clone #4, and YFP MH6556 Clone #4 (gifts from Dr. Stanger, University of Pennsylvania) were isolated from primary tumors of genetically engineered mouse model (Kras-G12D p53^{-/-} YFP Rosa) and cultured in DMEM/F12 + 10% fetal bovine serum (FBS) + 2 mM L-glutamine + 50 µg/ml Gentamycin. Human pancreatic cancer cell lines, Panc-1 (a gift from Dr. Faller, Boston University) and BxPC-3 (a gift from Dr. Stanger, University of Pennsylvania) were cultured in DMEM + 10% FBS + 1% Pen/strep and in RPMI1640 + 10% FBS + 1% Pen/Strep, respectively. Panc-1 and BxPC-3 were transduced with GFP lentivirus for visualization and quantification of the invasion area. Normal mouse pancreatic ductal epithelial cells (a gift from Dr. Rustgi, University of Pennsylvania) were cultured as previously described(41). Human umbilical vein endothelial cells (HUVECs, Lonza) were cultured in EGM-2 (Lonza). EGM-2 was used in all coculture experiments unless indicated otherwise. All cells in the study were routinely tested to confirm no mycoplasma contamination.

Device fabrication and 3D organotypic PDAC experiments. Our organotypic PDAC on-a-chip was comprised of two polydimethylsiloxane (PDMS) gaskets, cast from silicon wafer masters. The gaskets were bonded after plasma etching, treated with 0.1 mg/ml poly-L-lysine (Sigma) overnight and subsequently treated with 1% glutaraldehyde (Electron Microscopy Sciences). 2.5 mg/ml rat tail collagen I (Corning) was pipetted into the devices after 2 acupuncture needles of 300 µm diameter were inserted in the device. Retrieval of the needles after gelation left 2 hollow cylindrical channels suspended within the collagen interstitial matrix. The two channels generated by the acupuncture needles were either 500 µm apart or 1 mm apart from each other.

To quantify the invasion speed of PDAC cells in 3D, we used devices where two hollow channels, generated by acupuncture needles, were 1mm apart. Gradient characterization was also performed in device where the two channels were 1 mm apart. For screening experiment to identify the most robust

chemotactic agent for pancreatic cancer cells, we used devices when the two channels were also 1 mm apart. Monocyte chemoattractant protein 1 (MCP-1), Hepatocyte growth factor (HGF), Epidermal growth factor (EGF), Vascular endothelial growth factor (VEGF), basic Fibroblast growth factor (bFGF), and Stromal cell-derived factor 1 (SDF-1) were all used at 100 ng/ml into the source channel without endothelial cells. 20% FBS was deemed as the most effective chemoattractants to trigger invasion of pancreatic cancer cells when the source and sink channels were 1mm apart.

All other experiments were performed with devices where needles were 500 μ m apart from each other to facilitate tumor-vascular interactions in a shorter period of time. Of note, to maintain the similar gradient, since we reduced the distance between the two channels by half, the amount of FBS was also reduced by half to maintain the steepness of the FBS gradient (20% FBS was supplemented into the source channel when the two channels were 1mm apart, and 10% FBS was supplemented into the biomimetic blood vessel when the two channels were 500 μ m apart). In all cases, PDAC cells were seeded at 2×10^6 cells/ml in EBM-2 (Lonza) and HUVECs were seeded at 3×10^6 cells/ml in EGM-2 (Lonza) as previously described (18). Devices were placed on a platform rocker (Benchmark Scientific) as previously described (18).

One day after cell seeding, media in the blood vessel channel (EGM-2) was supplied with additional FBS (10% FBS for devices whose biomimetic blood vessel and pancreatic cancer duct were 500 μ m apart, and 20% FBS for devices whose biomimetic blood vessel and pancreatic cancer duct channel were 1 mm apart) to induce migration of PDAC cells. Media in the PDAC channel (EBM-2) was also refreshed the next day after cell seeding. The media in both biomimetic blood vessel (EGM-2 + 10% FBS) and pancreatic cancer duct channel (EBM-2) were refreshed daily to maintain the gradient of FBS over the entire course of the experiments.

For experiment to inhibit TGF β signaling with SB431542, the biomimetic blood vessel and pancreatic cancer duct were 500 μ m apart. SB431542 (Tocris) was administered at 5 μ M into both channels when the PDAC cells closely approached the endothelium. For activin inhibition experiment using follistatin, the

biomimetic blood vessel and pancreatic cancer duct were 500 μm apart. Follistatin (Peprtech) was administered at 200 ng/ml into both channels when the PDAC cells closely approached the endothelium. Medium supplemented with inhibitors was refreshed daily for both SB431542 and follistatin experiments.

Characterization of the gradient in 3D organotypic model. 21kDa fluorescein isothiocyanate (FITC-dextran) dextran (Sigma) was introduced into the biomimetic blood vessel at the concentration of 0.5mg/ml. We used devices whose channels were 1mm apart from each other. At 1hr, 4hr, and 24hr after FITC-dextran was added into the biomimetic blood vessel, we imaged a single focal plane using a 10x objective with spinning disk confocal microscope and acquired multiple overlapped positions along the distance between the biomimetic model and the pancreatic duct channel. Overlapped images were stitched, and we measured the intensity of FITC-dextran along a straight line between the two channels.

Cloning and virus production. ALK4, ALK5 and ALK7 were knocked out by using the LentiCRISPRv2 vector (Addgene). The two complementary oligos were listed in Table 1. The oligos were mixed at 1:1 ratio to a final concentration of 50 μM and annealed as followed: 37°C for 30 mins, 95°C for 5 mins, and then ramped down to 25°C at 5°C/min. All cloning products were confirmed by sequencing from QuintaraBio. For lentivirus production, HEK 293T/17 cells were transfected with three plasmids (15 μg lentiviral vector, 15 μg psPAX2, and 5 μg pMD2G), using the standard calcium phosphate precipitation method. Virus was harvested 24 hrs post transfection, filtered through 0.45 μm filter (Millipore), pelleted by PEG-it solution (System Biosciences), and resuspended in medium.

Western blot analysis. Total protein lysates were isolated using RIPA buffer (Cell Signaling). Proteins were fractionated by SDS-PAGE. Primary and secondary antibodies included rabbit anti-ALK5 antibody (Abcam, ab31013, 1:500), rabbit anti-ALK7 antibody (Abcam, ab65088, 1:1000), rabbit anti-ALK4 antibody (Abcam, ab109300, 1:1000), rabbit anti-GAPDH (Cell Signaling, 5174s, 1:10000), rabbit anti-Smad2 (Cell Signaling, 5339S, 1:1000), rabbit anti-phospho-Smad2 (Cell Signaling, 3108S, 1:500) and HRP-linked anti-rabbit IgG antibody (Cell Signaling, 7074, 1:5000). All primary and secondary antibodies

were blocked in 5% milk in TBS + 0.1% Tween-20 except for anti-phospho-Smad2 antibody in 5% BSA in TBS + 0.1% Tween-20.

Immunofluorescence staining in 2D cultures. Samples were fixed with 4% paraformaldehyde (PFA) and permeated with 0.1% Triton-X. Then the samples were blocked with 3% bovine serum albumin (BSA) in phosphate buffered saline (PBS), and subsequently incubated with primary antibodies and secondary antibodies in the blocking buffer at room temperature. The primary antibodies include anti-CD31 (Dako, M0823, 1:200), fluorescein isothiocyanate (FITC)-conjugated anti-GFP (Abcam, ab6662, 1:500), anti-cleaved caspase-3 (Cell Signaling, 9961S, 1:500), and DAPI (Sigma, 1:500). All secondary antibodies (Invitrogen) were used at 1:1000 in the same blocking buffer. The samples were rinsed with PBS 3 times between antibody incubation steps. FITC-conjugated anti-GFP antibody was used to stain YFP cancer cells.

Immunofluorescence staining and imaging in 3D organotypic model. Devices were fixed with 4% PFA, permeated and blocked with 3% BSA overnight at 4°C. Primary antibodies detecting CD31 (Dako, M0823, 1:200), GFP (Abcam, ab6662, 1:500), cleaved caspase 3 (Cell Signaling, 9961S, 1:500), and DAPI (Sigma, 1:500) were all incubated in blocking buffer overnight at 4°C. FITC-conjugated antibody against GFP was used to stain the YFP cancer cells. Primary antibodies were washed overnight using PBS at 4°C. Secondary antibodies (all from Invitrogen, 1:500) were subsequently incubated in blocking buffer overnight at 4°C, and the devices were washed to remove fluorescent background before confocal microscopy. Confocal images were acquired with an Axiovert 200M inverted microscope (Zeiss) equipped with an CSU10 spinning disk confocal scan head (Yokogawa Electric Corporation), and an Evolve EMCCD camera (Photometrics).

Quantification of the invasion speed of tumor cells in 3D organotypic model. The devices were imaged live using bright field microscopy, Nikon TE200 with 10x air objective. Multiple overlapping images were acquired and stitched together to obtain the entire pancreatic duct channel. A custom Matlab code was used to track the distance from the tip of each tumor cell sprouts to the pancreatic duct. The average of the distance was calculated and reported at several time points.

EdU staining in 3D organotypic model. Cell proliferation in 3D organotypic model with or without FBS was assessed by using Click-iT EdU Imaging kits (Invitrogen). 3D organotypic model was cultured with or without FBS for 2 or 5 days and 10 μ M EdU was incorporated at Day 2 and Day 5 respectively. After 30 min incorporation of EdU, the solution was removed and the cells in the chip were fixed with 4% PFA for 30 min. After fixation the device was permeabilized with 0.5% Triton in PBS for 1 hour. EdU detection was performed following the protocol provided by the vendor. Briefly, 1X Click-iT[®] EdU buffer additive and Click-iT reaction cocktail were prepared. The Click-iT[®] reaction was initiated within 15 minutes of cocktail preparation by adding 300 μ l of the reaction cocktail to the device. Reaction was done for 4 hours on a rocker and the Click-iT reagent was removed and washed by 3% BSA in PBS. After that, antibody staining for anti-GFP (1:500 in 3% BSA) and DAPI (1:500 in 3% BSA) were performed for co-staining.

Quantification of the area of biomimetic blood vessel replaced by tumor cells in 3D organotypic model. The devices were fixed and stained as discussed above. To capture the entire biomimetic blood vessel, we utilized 10x air objective and imaged several overlapping areas of the biomimetic blood vessel until tumor cells were no longer visualized on the biomimetic blood vessels. Using ImageJ, we stitched these overlapping stack images together. Then we individually projected the top half and bottom half of the vessels. Using a custom Matlab code, we traced the area of the blood vessel that was replaced by tumor cells for both the top half and the bottom half of the biomimetic blood vessel. The total tumor replaced blood vessel was the sum of the tumor replaced areas from the bottom half and top half of the biomimetic blood vessel. Our biomimetic blood vessels were generated by acupuncture needles with 300 μ m diameter and 6mm in length, which gave us a total surface area of the blood vessel as 5.65mm². The % of tumor replaced vessel area was calculated by dividing the tumor replaced vessel area by the initial biomimetic blood vessel area of 5.65mm². Representative images of vessel areas that were replaced by tumor cells for both SB431542 experiment and follistatin experiment are provided in fig. S8.

Movie rendering for endothelial cell-ablated blood vessel in 3D organotypic model. The devices were fixed and stained as discussed above. To enable us to perform 3D rendering, we utilized a water immersion 40x objective to image through the gel and capture the bottom half of the biomimetic blood

vessel whose endothelial cells were partially ablated by the tumor cells (the working distance of the objective was not able to fully capture the upper part of the biomimetic blood vessel that was deep inside the gel). Confocal images were acquired with an Axiovert 200M inverted microscope (Zeiss) equipped with an CSU10 spinning disk confocal scan head (Yokogawa Electric Corporation), and an Evolve EMCCD camera (Photometrics). Several overlapped positions were imaged and stitched together using ImageJ. Finally, the stitched images were 3D rendered using Imaris (Bitplane).

PDAC vascular invasion in 2D patterned coculture invasion assay. Annulus rings were fabricated using biopsy hole punches (2 mm and 3.5 mm diameter) from a PDMS slab. The annulus rings were placed in the center of wells in a 24-well plate. 10,000 PDAC cells were seeded inside the annulus ring while HUVECs were subsequently seeded at 150,000 cells outside the annulus ring. The annulus rings were peeled off the next day, and the cells were allowed to grow for 2 days until the two cell types were in contact all around the tumor cell patterns. The experiment was then initiated, and images were acquired at $t=0$. To quantify the invasion area of PDAC cells, multiple overlapping images of YFP PDAC cell islands were imaged using TE200 microscope (Nikon). The overlapping images were stitched, and the PDAC invasion area was quantified using a custom Matlab code to track the area of the tumor cell pattern as discussed below. SB431542 was used at 5 μM . Follistatin (Peprotech) was administered at 80 ng/ml. Aphidicolin was used at 0.5 $\mu\text{g/ml}$. All inhibitors were refreshed daily.

For experiment with ALK7 knockout cells, the same number of cells was plated for both ALK7 KO and Scramble cells. After the annulus rings were removed, we allowed the tumor cells to grow into contact with the endothelial cells in all around the tumor cell patterns for 4 days.

Quantification of invasion area in 2D patterned coculture invasion assay. At time $t=0$, defined as the timepoint when the fluorescently-labelled cancer cells and non-labelled endothelial cells came into contact (2 days after the annulus was peeled off in all cases), we took multiple overlapping images of tumor cell pattern with Nikon TE200. Using ImageJ, the overlapping images were stitched together to acquire the entire patterned of tumor cells. Using a custom Matlab code, the edge of the tumor pattern

was tracked, and the total area of the tumor pattern was computed as the initial tumor area. This procedure was repeated at later time points. The invasion area at each time point was defined as the difference between the tumor area at each time point and the initial tumor area. Representative images of tumor cell patterns at several time points when the coculture was treated with DMSO vs SB431542 were provided in fig. S9.

Conditioned medium experiment and quantification of active caspase with bioluminescence in conditioned medium experiment. Endothelial cells were plated into wells of 96 well plate at 15000-17000 cells/well to form a monolayer overnight. EGM-2 was added into the culture of tumor cells at 80% confluency overnight. A separate dish without tumor cells was also prepared with the same amount of EGM-2 to serve as a control medium. The next day, the tumor conditioned medium in tumor cells and medium from control dish were collected and immediately added into the monolayer of endothelial cells. The following day, active caspase3/7 bioluminescence kit (Promega) reagent was added into the well per the instruction manual to measure the bioluminescent signal intensity produced by active caspases.

Quantification of cleaved caspase-3 signal intensity in 2D patterned coculture assay. Tumor PD7591 and endothelial cells were plated as discussed above in the 2D patterned coculture assay. 3 days after the annulus was removed and the two cells came into contact, we fixed the cells with 4% paraformaldehyde and performed staining for CD31, and cleaved caspase-3. Anti-GFP antibody was also used to stain YFP PD7591. For each pattern of tumor cell island, we imaged 4 random images at four different corners with a 10x objective using TE200 microscope (TE200). For each image, using a custom Matlab code, we traced the interface between tumor and endothelial cells and drew the boundary line between the tumor cells and endothelial cells. At each location along the boundary line, we acquired the caspase signal intensity as a function of distance up to 300 μm away from the boundary line. Then we average the signal intensity of caspase as a function of each distance (0-300 μm) away from the boundary line. A total of 5 patterns from 5 individual experiments were used for each condition.

Mouse tumor model. Two million of PD7591 pancreatic cancer cells were resuspended in 1:1 mixture of cancer cell growth medium and high protein concentrated Matrigel (Corning) on ice for a total volume of 100 μ L and subcutaneously injected into an athymic nude mouse (Taconic, NCr-nu/nu, 4-5 week, female) by using insulin syringes. Mice were placed under anesthesia with standard isoflurane (1-4%) inhalation during tumor injection. Mice were monitored daily after the tumor injection. Long axis, A, and short axis, B, of the tumor were measured with a digital caliper every 2 days to calculate the tumor volume as $0.52 \times (A \times B^2)$. Tumors were allowed to grow to a maximum volume of 2000 mm^3 in all cases in consideration for the animals' welfare. All procedures were performed in a sterile environment of a laminar flow cabinet housed in the Charles River Campus animal facility at Boston University. After the experiments were complete, the animals were euthanized using carbon dioxide followed by a cervical dislocation, and the tumors were excised to examine tumor microenvironment and tumor invasion to blood vessels. In some instances, to acquire the staining of Collagen IV in the basement membrane surrounding the blood vessels within the tumors, we resuspended PD7591 in cancer growth media without Matrigel and followed the same procedure described above. Exclusion of Matrigel during tumor cell injection ensured the presence of Collagen IV was from the blood vessels rather than from the basement membrane protein-rich Matrigel. For SB431542 treatment, SB431542 (Tocris) was solubilized in DMSO at 20 mg/ml. At day 9 of tumor outgrowth, 10 mice were randomly assigned into 2 groups (5 mice/group). We administered SB431542 intraperitoneally using insulin syringes into one group of mice at 25 mg/kg/day for 7 days, and vehicle control (DMSO) into the other group. Mice were sacrificed as described above after the experiments were complete. No statistical method was used to pre-determine the sample size. All animal procedures were performed at the Charles River campus animal facility at Boston University under a protocol approved by the institutional IACUC. All experiments in this study conformed to the "Guide for the Care and Use of Laboratory Animals", published by the United States National Institutes of Health (Eighth Edition, 2011).

Genetically engineered mouse model. Kras^{LSL-G12D}; p53^{L/+}; Pdx1-cre; Rosa26^{YFP/YFP} (KPCY) tissues were a kind gift from Dr. Ben Stanger's laboratory (University of Pennsylvania). The model has been described previously (Rhim et al, 2012). Briefly, mice were palpated and examined for evidence of

morbidity twice per week. Tumor bearing animals were sacrificed when morbid and primary pancreatic tumors were collected from mice aged 14-30 weeks. Tissues were flash-frozen in OCT and subsequently processed for immunofluorescent staining as discussed below.

Tumor tissue processing and immunofluorescence staining. Excised tumors were rinsed in PBS, and fixed in 4% PFA for 18 hrs at room temperature, then stored in 100% methanol at -20°C. For immunofluorescence, fixed tumors were placed in 30% sucrose solution in PBS for 2-3 days at 4°C, and frozen in Tissue-Tek Optimal Cutting Temperature (O.C.T.) compound (Sakura). Sections of 10- μ m thickness were cut at -20°C. For sections from the GEMM tissue, antigen retrieval was done in sodium citrate buffer (10mM, pH6) at 98°C for 30 minutes. After blocking with 5% normal goat serum (Jackson ImmunoResearch) in PBST (1X PBS + 0.3% Triton) overnight at 4°C, the sections were treated with primary antibodies overnight at 4°C: rabbit anti-cleaved caspase-3 (Cell Signaling, 9961S, 1:100), rat anti-mouse CD31 (BD Pharmingen, 553370, 1:100), rabbit anti-collagen IV (Abcam, ab6586, 1:100), rat anti-mouse endomucin (Santa-Cruz, sc-65495, 1:100). Sections were washed in PBST overnight at 4°C and subsequently incubated with DAPI (4',6-diamidino-2-phenylindole, 1:10000, Roche) and secondary antibodies overnight at 4°C: fluorescein isothiocyanate (FITC)-conjugated goat anti-GFP antibody (Abcam, ab6662, 1:500), rhodamine-conjugated goat anti-rat antibody (Jackson ImmunoResearch, 1:500), Alexa 647-conjugated goat anti-rabbit antibody (Jackson ImmunoResearch, 1:500). Samples were washed and mounted with the ProLong Gold anti-fade reagent (Invitrogen). Fluorescent images were acquired with Leica TCS SP8 confocal microscope.

Quantification of cleaved caspase-3 and CD31 signal in tumor tissue sections: To minimize variability in signal intensity for Caspase 3 and CD31 across tissue sections and samples, all protocols to fix, process, stain and image the tumors were kept constant. To the extent possible, samples were sectioned, stained and imaged simultaneously to ensure that no processing artifacts could arise between different samples. All tumors were imaged with the same microscopy settings (i.e. 10x objective, field of view of 897.8 μ m x 670.8 μ m and fixed laser intensities) and camera acquisition settings to ensure proper comparison between different sections. For the *in vivo* studies with SB431542, each experimental group had a total of 85 images from 5 mice/group (17 images per mice). To quantify the CD31 signal intensity,

we performed the same level of thresholding across all the images using ImageJ on the CD31 channel to eliminate background signal. The total signal intensity of CD31 after thresholding was analyzed using ImageJ for each field of view. We then normalized the CD31 signal intensity to the average CD31 signal intensity in DMSO 1 week to enable us to compare across 1 week and 2 week conditions. For cleaved caspase-3 signal analysis, we used the same thresholding level for all images of cleaved caspase-3 channel across DMSO and SB431542 conditions to eliminate background signal. Then we subjected the images to our custom Matlab code to isolate cleaved caspase-3 signal that overlapped with the CD31 signal (previously thresholded during CD31 analysis using the same level for all images in DMSO and SB431542 conditions). The sum of caspase signal in CD31 positive endothelial cells was used to calculate the total cleaved caspase-3 signal in endothelial cells for each image or field of view. To allow comparison between different conditions, the cleaved caspase-3 signal intensity was normalized to the DMSO control sample at 1 week.

For the ALK7 knock out PDAC implantation experiments, each experimental group had a total of 25 images (5 mice/group and 5 images per mice). To eliminate background signal in the CD31 channel, the threshold was kept constant across the experimental groups using ImageJ. After thresholding, the total CD31 signal intensity was analyzed in ImageJ for each image. For cleaved caspase-3 signal analysis, we performed the same analysis as described above for the SB431542 experiments, with the difference that the data for ALK7 KO condition was normalized to the Scramble condition. A schematic illustrating the steps to perform analysis for CD31 signal intensity and cleaved caspase-3 signal is provided in fig. S10.

Statistical analysis. Independent sample populations were compared using unpaired, two-tailed Student's t-test with a normal distribution assumption. *P < 0.05 was the threshold for statistical significance. * denotes p-value < 0.05, ** denotes p-value < 0.01, and *** denotes p-value < 0.001. All information regarding the number of experimental repeats and sample sizes were included in figure legends. All data points on the graphs represent average values, and error bars depict SEM.